

**Title: Manoeuvring of Micro Robots using External
Magnetic Fields**

A DISSERTATION SUBMITTED IN PARTIAL FULFILMENT
FOR THE DEGREE OF

Master of Technology

IN THE
FACULTY OF ENGINEERING

BY

SAMEER SUHAS PUJARI

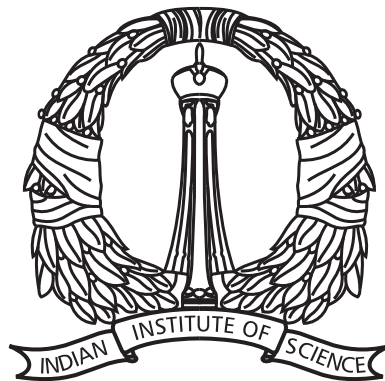
(SR No- 05-08-02-10-51-20-1-18768)

S SURYA TEJA

(SR No- 05-08-02-10-51-20-1-18188)

GUIDED BY

PROF. G. K. ANANTHASURESH
PROF. KAUSHIK CHATTERJEE



CENTER FOR PRODUCT DESIGN AND MANUFACTURING
INDIAN INSTITUTE OF SCIENCE, BANGALORE

JUNE 2022

COPYRIGHT © 2022 IISc
ALL RIGHTS RESERVED

Acknowledgements

My deepest gratitude is to my advisors, **Prof. G.K. Ananthasuresh** and **Prof. Kaushik Chatterjee**. I have been amazingly fortunate to have advisors who supported me throughout the project. Their support helped me pass through all the challenges and difficulties I encountered.

A special thanks to **Sudhanva Bhat** for the valuable guidance throughout the project.

I want to thank my family, friends, and the one above all of us, the omnipresent God, for their support. Finally, I would like to thank my families of M2D2, Biomaterials, CPDM, and IISc.

Abstract

In this dissertation, a local magnetic field generating system for microrobot actuation is designed and modelled. Robots ranging from 4-8mm diameter are controlled to move on the 2D workspace. The field produced by the coils is experimentally validated and a new design of robot is shown, where the bot can be manipulated even when it is not in direct contact with the 2D platform. A camera based position feedback system is designed to get the present location of the bot, and this information is sent to the path planning algorithm, where it decides which is the next best position for the bot to reach, and this information is sent to Arduino to actuate those particular coils to reach the next position. Different kinds of movements are achieved where the bot was moved from (a) centre of the coil to corner of the coil and (b) corner of the coil to centre of the coil and the strategies employed to move the bot in that particular format are discussed. Using local field control strategy, multiple robot control is achieved, where two bots motion are controlled independently. Finally an attempt is made to re orient a part placed on the 2D grid, with the help of a microrobot.

Contents

Abstract	v
Table of Contents	vii
List of Figures	xi
1 INTRODUCTION	1
1.1 Motivation	1
1.2 Background	1
1.2.1 Thermal Actuation	2
1.2.2 Electrostatic Actuation	2
1.2.3 Biological Actuation	2
1.2.4 Optical Actuation	2
1.2.5 Electromagnetic Actuation	2
1.2.6 Magnetic actuation	3
1.3 Objective	3
1.4 Contribution	4
2 SYSTEM DESIGN	5
2.1 Details of the Micro Robot	5
2.2 Details of the Coil Design	7
2.2.1 Magnetic field of a straight wire segment with finite length	7
2.2.2 Gradient of Magnetic field of a straight wire segment with finite length	10
2.2.3 Magnetic force generated by straight wire segment with finite length on the micro bot	11
2.2.4 Magnetic Field due to a rectangular coil	13
2.2.5 Variation of Force acting on the micro bot	14

2.2.5.1	Changing the current in the coils	14
2.2.5.2	Increasing no. of turns in the same plane	16
2.2.5.3	Increasing no. of turns in the same plane	17
2.2.5.4	Height from PCB	17
2.2.6	Design Choice of Coil on PCB	18
2.2.7	Comparison of Forces acting on the type of material of the micro robot	18
2.2.8	Final PCB Design	19
2.2.9	Losses in the Designed coil	20
2.3	Experimental Verification	21

3 EXPERIMENTAL TEST-BED DESIGN 23

3.1	COMPONENTS	23
3.1.1	PCB	23
3.1.2	Robot	25
3.1.3	Electronics	25
3.1.4	Voltage Control Driver IC- MX1919	26
3.1.4.1	Pin Diagram	26
3.1.4.2	Technical Specifications	26
3.1.5	PWM Driver IC- PCA 9685	27
3.1.5.1	Pin Diagram	27
3.1.5.2	Library reference commands	27
3.1.6	Power Supply	28
3.1.7	Camera	28
3.1.8	Controller	28
3.2	CONNECTION OF COMPONENTS	29
3.3	PICTURE OF FINAL SETUP	31

4 IMAGE PROCESSING 33

4.1	OpenCV - An Open Source Computer Vision Library	33
4.1.1	Identifying the edges of the coil array	33
4.1.2	Image Preprocessing	34
4.1.3	Identifying robots location	35
4.1.3.1	Hough Transform	35

4.1.3.2	Finding points on the robot contour and averaging to get the Center	36
4.2	Identifying coil centers and corners	36
4.2.1	Colour Detection of robot	38
5	ROBOT MOTION CONTROL	41
5.1	Local equilibrium point modeling	41
5.2	Types of possible movements	42
5.2.1	Corner to Center movement	42
5.2.2	Center to Corner movement	44
5.3	Path Planning	44
6	VALIDATION EXPERIMENTS	47
6.1	Single Robot Manoeuvring experiments	47
6.2	Multi Robot Manoeuvring experiments	49
6.3	Application- Part re-orientation	49
7	FUTURE WORK	51
8	REFERENCE- GitHub Link	53
	Bibliography	54

List of Tables

2.1	Dimensions of Micro Robot	6
2.2	Change in range of force with respect to change in current through the coils . .	15
2.3	range of force and influencing distance vs the no.of turns	16
2.4	No. of layers increases vs the range of force increases	17
2.5	PCB and Coil Specifications	20
4.1	BGR and HSV ranges used	38
4.2	Hue ranges for different colors used	39

List of Figures

2.1	Cylindrical Micro Robot and it's dimensions	7
2.2	Conductor carrying current I, placed at a distance 'a' from origin parallel to Y-axis on X-Y Plane	8
2.3	Conductor carrying current I, placed at a distance 'a' from origin parallel to X-axis on X-Y Plane	9
2.4	Analytical Result of Variation in Field (wire is into the plane)	9
2.5	FEM Model Based variation of Magnetic Flux Density on COMSOL	10
2.6	Variation of Gradient of Field (B_x) along X axis at height $z = 150 \mu\text{m}$	11
2.7	Variation of Gradient of Field (B_x) along X axis at height $z = 150 \mu\text{m}$	12
2.8	Magnetic forces acting on the cylindrical bot	12
2.9	Comparison of $F_{mag, x}$ and $F_{mag, z}$	13
2.10	Different types of traces on PCB	13
2.11	Analytical Result of Variation of Force on bot w.r.t Current	15
2.12	Analytical Result of Variation of Force on bot w.r.t No. of Turns in same plane for $I = 0.7\text{A}$	16
2.13	Analytical Result of Variation of Force on bot w.r.t No. of Layers of PCB, for $I = 0.7\text{A}$	17
2.14	Analytical Result of Variation of Force on bot w.r.t Height away from PCB for $I = 0.7\text{A}$	18
2.15	Comparison of Analytical Result of Variation of Force on bot w.r.t type of material $I = 0.7\text{A}$, * a) Permanent Magnet b) Ferro Magnet	19
2.16	PCB Design	20
2.17	Experimental setup for field measurement	21
2.18	Simulink model replicating the dynamics of the system	22
2.19	Robot repulsion and attraction in Simulink model	22
3.1	Zoomed in view of a single coil	23

3.2	Final PCB Design with an 8×8 grid of spiral coils	24
3.3	Permanent magnet robot and its dimensions	25
3.4	MX1919 Based Motor Driver Module – 2.5A	26
3.5	Adafruit 16- channel 12-bit PWM Driver	27
3.6	Simplified Setup Schematic	29
3.7	Setup Schematic with Camera Feedback	30
3.8	Final System	31
4.1	Figure shows 4 corners of the working area with Yellow circles and working area is highlighted in Red	34
4.2	Equation of circle	35
4.3	Center waypoints in yellow and Corner waypoints in pink	38
5.1	Forces acting on the robot depending on the direction of the current and position of robot	41
5.2	Overall Force generated by the coil along X-axis. Coil range -1 mm to 1 mm	42
5.3	Coil required to attract the robot from corner to center, Green coil- Attractive field	43
5.4	Corner to Center movement * Red shaded coil is turned on to repel the robot and yellow shaded coil is turned on to attract	43
5.5	Coils required to attract the robot towards the corner. * Green coil- Attractive field, Red coil- Repulsive field	44
5.6	Center to Corner movement * Red shaded coil is turned on to repel and yellow shaded coil is turned on to attract	44
5.7	Waypoints for A^* algorithm consist of each coils center and corner positions, all marked with an "x"	45
6.1	Corner to Center movement * Red shaded coil is turned on to repel the robot and yellow shaded coil is turned on to attract	48
6.2	Coils required to attract the robot towards the corner. * Green coil- Attractive field, Red coil- Repulsive field. Planned Path- Black, Actual Path- Red	48
6.3	Coils required to attract the robot towards the corner. * Green coil- Attractive field, Red coil- Repulsive field	49
6.4	Initial and final picture of part-reorientation experiment	50

Chapter 1

INTRODUCTION

1.1 Motivation

Micro-size mobile robotics is the field of robotics where the design, fabrication, and manipulation of the robotic agents are in the range of micrometers. The dominant forces acting on this scale of robots are surface forces such as friction, adhesion, drag, and surface tension because the inertial and buoyancy forces are negligible compared to them[1]. Typically, robots are equipped with sensors, controllers, and end effectors to realize their full potential by augmenting their capabilities beyond just locomotion. As the robot's footprint is on a micro-scale, it is challenging to accommodate such onboard power, sensors, communication cables, and the controller circuit directly on the robot. Hence using external control and actuation system is essential to reduce these challenges created by the robot's size.

Micro assembly, micro orientation, and micromanipulation methods improve hybrid MEMS's manufacturability, such as integrating solid-state ICs with MEMS sensors and actuators [2]. The critical requirements of such a micro-assembly system are high precision and throughput at a low cost, which can be achieved through parallel manipulation and modular system designs [3]. Meso-scale agents have the potential to provide assistance in minimally invasive procedures that benefits patients. Traditionally, these procedures should comply with reduced infection risk, recovery time, and medical complications [1][4][5].

1.2 Background

The different types of power and actuation mechanisms that can be applied to mobile micro-robots include thermal [6], piezoelectric [7], electrostatic [8], biological [9], and optical [10], electromagnetic [11][12].

1.2.1 Thermal Actuation

Thermally-induced curvature of legs of a microrobot leads to stepwise translation on low frictional surfaces in [6]. However, they can generate only the pN level of forces during actuation.

1.2.2 Electrostatic Actuation

Phase modulation and Amplitude modulation of voltages were two techniques applied on an array of electrodes that proved a powerful approach to controlling the Dielectrophoretic force acting on the particle provided by the induced field. Execution of parallel manipulation of several particles and even the swapping of particles on the parallel electrode array were shown in [8]. This electrostatic control scaled favorably with size due to matching scaling of adhesive friction forces and electrostatic friction, which aided in successful actuation. Even though parallel manipulation of particles was achieved, Dielectrophoresis is a complex procedure to manipulate particles as electroosmosis, thermally induced flow, and electrolysis was observed that damage the costly electrode arrays, etc.

1.2.3 Biological Actuation

This process uses microorganisms such as bacteria or algae to actuate microrobots. The microorganisms can convert their chemical energy to mechanical energy [9]. Many bio-hybrid microrobots have been developed in the past decade. However, they have key challenges such as fabrication efficiency and require large swarms of microorganisms to carry sufficient payloads.

1.2.4 Optical Actuation

Optical manipulation methods were developed recently where a single laser beam is split into multiple paths with the help of a spatial light modulator or high-speed mirror technology [10]. Optical manipulation is achieved using holographic optical tweezers, which function as special robot end-effectors that can manipulate a single or a group of microparticles. However, the parts that can be controlled are limited to tens of nanometres to tens of micrometers.

1.2.5 Electromagnetic Actuation

From the past decade, several electromagnetic systems have been designed to control untethered mobile microrobots [11][13]. The microrobots used with these systems are made of either permanent magnetic, ferromagnetic, or paramagnetic material, and their designs are, in most cases, planar magnetic bodies. Any magnetic microrobot placed in the workspace of the electromagnetic control system will experience torque and force due to the applied magnetic field. Thus, the microrobots can be controlled by modulating the magnitude and direction of current passing through the magnetic coils surrounding the workspace. Installing a micro robot using

a magnetic field is possible on various surfaces. In [14], microrobots were actuated on dry surfaces using oscillating magnetic fields. Another approach is to use magnetic field gradients to pull the microrobots towards the coils. Such systems usually rely on an iron core to magnify the field gradients in the workspace. Several magnetic actuation systems [12][15] can control the position and orientation of the robots without oscillating fields.

1.2.6 Magnetic actuation

Magnetic actuation is widely used in micro-robotic actuation due to its ability to penetrate the field through a wide range of materials. They are also relatively strong compared to other microrobot actuation methods. It is also easy to integrate magnetic materials into existing microfabrication methods[16]. Several neodymium micro magnets are available commercially in the market.

In Magnetic Actuation, two possible strategies for manipulating the micro robot are based on the arrangement of coils. The first kind is called the global field control strategy, where the manipulation area is enclosed by the coils, providing a limited workspace where the micro-robot can be controlled. This strategy changes the field throughout the workspace and requires robust magnetic systems for larger workspaces. Here every magnetic bot in the workspace is influenced by the identical coils. Hence independent control of multiple magnetic bots is challenging. Mag- μ Bot [17], a permanent magnet actuated by six air coils placed as the faces of a cube. To obtain individual control of the microrobots using a global magnetic field, the heterogeneity of magnetic microrobots smaller than 1 mm in all directions was exploited [13]. It was observed that the non-uniformity of the microrobot's magnetic properties allowed them to respond differently to the applied global field, but their motions were still coupled. This approach also does not scale well to handle large numbers of microrobots.

The second kind is called the local field control strategy, where the arrangement of the coils is in the form of a planar array, and this array can be extended to a larger area just by adding more coils. In this strategy, every coil affects only a small portion of the workspace. Therefore relatively smaller electromagnets can be used, unlike global field control. Here every magnetic bot is affected by a different set of coils in the workspace; hence independent control of multiple magnetic bots is possible. The limitation to this strategy is that the bot manipulation is restricted to a 2D platform. Therefore, instead of using a single global magnetic field for multi-robot control, multiple local magnetic fields can be utilized to control multiple microrobot.

1.3 Objective

This dissertation aims to design and evaluate a 2D platform (PCB) with a grid of coils to generate local magnetic fields; on the platform, multiple microrobot are placed, and their position is controlled independently using these external fields.

1.4 Contribution

1. Designing a novel local magnetic field generating system.
2. Modeling of local magnetic fields generated by the planar coils.
3. Development of a platform to host multiple local magnetic fields generating systems and control multiple bots.
4. Designing a Simscape model to understand the system dynamics based on analytical equations.
5. New microrobot design, showing that the bot need not be in direct contact with the 2D platform.
6. Path planning of robots to avoid obstacles, considering other robots in the workspace.
7. Position-based control of microrobot in the workspace to perform part re-orientation tasks.

Chapter 2

SYSTEM DESIGN

The microbot is to be controlled using an external magnetic field generated by a 2D grid of coils, and these coils produce a non-uniform magnetic field which varies across space. The force acting on the micro robot due to a non-uniform magnetic field B_{ext} (x, y, z) is given by

$$F_{mag} = v(M \cdot \nabla) B_{ext} = v \begin{pmatrix} M_x \frac{\delta B_x}{\delta x} + M_y \frac{\delta B_x}{\delta y} + M_z \frac{\delta B_x}{\delta z} \\ M_x \frac{\delta B_y}{\delta x} + M_y \frac{\delta B_y}{\delta y} + M_z \frac{\delta B_y}{\delta z} \\ M_x \frac{\delta B_z}{\delta x} + M_y \frac{\delta B_z}{\delta y} + M_z \frac{\delta B_z}{\delta z} \end{pmatrix} \quad (2.1)$$

where v is the volume of the micro robot, M is the Magnetization of the micro robot and B_{ext} (x, y, z) is the external magnetic field generated by the grid of coils in space. The Magnetization M (M_x, M_y, M_z) is the magnetic dipole moment(m) per unit volume of the micro robot. The magnetic dipole moment is given by the product of loop current and loop area in the direction of loop area vector. The following equations show the relation between Magnetization and magnetic dipole moment

$$M = \frac{dm}{dv} \quad (2.2)$$

$$m = LoopCurrent * AreaofLoop \quad (2.3)$$

It is found that the Magnetization also depends on the type of material of the micro robot.

2.1 Details of the Micro Robot

The type of material which responds to the applied magnetic field can either be a permanent magnet or a ferromagnet. In the case of a permanent magnet, the force applied depends on the current direction, as the magnet can attract for a given direction of current and repel when the current is sent in the opposite direction through the coils. The ferromagnet always tries to align its magnetic domain in the direction of current field applied, hence the ferromagnet always gets attracted to the coil, even when there is a change in current direction.

Height of Bot	0.9 mm
Radius of Bot	2- 4 mm
Volume of Bot = $\pi * r^2 * h$	11.30 – 45.23 mm ³
Density of Permanent/Ferro Magnet	7500 kg/m ³ (Considering Nd-FeB)
Mass of Micro Robot	84.83 - 339.93 - μ g

Table 2.1: Dimensions of Micro Robot

As explained earlier the Magnetization of the micro robot is also dependent on the type of material, and we have two materials, namely, permanent magnet and a ferromagnet. In case of a permanent magnet (hard magnetic materials), Magnetization is considered to be constant, because the field generated by the coils is very low that it is not sufficient to demagnetize such magnets, whereas in ferromagnet Magnetization is dependent on the external field generated by the coil and is given by

$$M = \frac{\chi_m B_{ext}}{\mu_0(1 + \chi_m)} \quad (2.4)$$

where χ_m is the magnetic susceptibility of the medium, in which the magnetic field is to be calculated and $\mu_0 = 4 \times 10^{-7}$ is the permeability of free space.

Both the ferromagnets and permanent magnets are available in different basic geometries such as a cube, sphere and a cylinder. In all the experiments we have done, we have chosen a cylindrical shaped micro robot because of the following reasons

1. As the base of a cylinder is flat, it can be easily manoeuvred and controlled on a 2D platform, unlike a sphere
2. The Magnetization of cylindrical micro robot is maximum along the axis of cylinder (M_z) which makes it a better choice, unlike a cube. The force magnitude depends on the magnetization, so for a micro robot having different magnetization along different sides will make it difficult to control
3. The cylindrical micro robots are readily available in various dimensions in the market

The dimensions and specifications of the Micro robot considered are shown in the table below and can be seen in the figure 2.1.

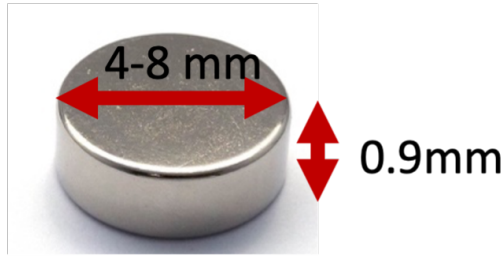


Figure 2.1: Cylindrical Micro Robot and it's dimensions

2.2 Details of the Coil Design

The force acting on the micro robot to manoeuvre on 2D platform is dependent on the magnitude of the external magnetic flux density $B_{ext}(x, y, z)$ generated by the coils and on the Gradient of the external magnetic flux density. The fundamental law of electromagnetism which describes the magnetic field generated by a current-carrying conductor is the Biot-Savart's Law, which is given by the equation,

$$dB = \frac{\mu_0(I dl \times \hat{R})}{4\pi R^2} \quad (2.5)$$

where I is the current flowing through the current element of length dl , which generates dB field at a point P which is at distance \hat{R} from origin. The 2D grid of coils can be modelled as a multiple single-segment wires arranged in parallel to the X or Y axis of the workspace. Later these segments can be connected to current controllers through traces, and these traces will be far away from the workspace so that it is assumed that their generated magnetic field does not affect the magnetic field in the workspace.

2.2.1 Magnetic field of a straight wire segment with finite length

Consider, a current wire of finite length (A – B), carrying a Current 'I' is placed on the X-Y plane and parallel to the Y-axis, at a distance 'a' from origin as shown in figure 2.2. By applying Biot – Savart's Law, we can calculate the magnetic flux density $B_{ext} = [B_x, B_y, B_z]$ at any point in space P (x, y, z) as

$$B_x = \frac{\mu_0 z I}{4[(a-x)^2 + z^2]} \times \left[\frac{y_2 - y}{\sqrt{(y_2 - y)^2 + (a-x)^2 + z^2}} - \frac{y_1 - y}{\sqrt{(y_1 - y)^2 + (a-x)^2 + z^2}} \right] \quad (2.6)$$

$$B_y = 0 \quad (2.7)$$

$$B_z = \frac{-\mu_0(a-x)I}{4\pi[(a-x)^2 + z^2]} \times \left[\frac{y_2 - y}{\sqrt{(y_2 - y)^2 + (a-x)^2 + z^2}} - \frac{y_1 - y}{\sqrt{(y_1 - y)^2 + (a-x)^2 + z^2}} \right] \quad (2.8)$$

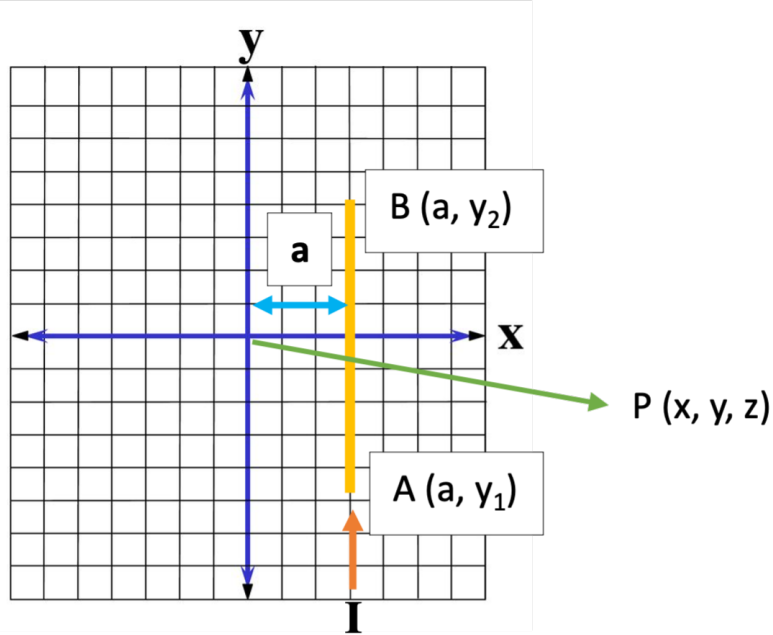


Figure 2.2: Conductor carrying current I , placed at a distance ‘ a ’ from origin parallel to Y-axis on X-Y Plane

Similarly, a current wire of finite length (A – B), carrying a Current ‘ I ’ is placed on the X-Y plane and parallel to X-axis, at a distance ‘ a ’ from origin as shown in figure 2.3. By applying Biot – Savart’s Law, we can calculate the magnetic flux density $B_{ext} = [B_x, B_y, B_z]$ at any point in space $P(x, y, z)$ as

$$B_x = 0 \quad (2.9)$$

$$B_y = \frac{-\mu_0 z I}{4\pi[(a-y)^2 + z^2]} \times \left[\frac{x_2 - x}{\sqrt{(x_2 - x)^2 + (a-y)^2 + z^2}} - \frac{x_1 - x}{\sqrt{(x_1 - x)^2 + (a-y)^2 + z^2}} \right] \quad (2.10)$$

$$B_z = \frac{-\mu_0(a-y) I}{4\pi[(a-y)^2 + z^2]} \times \left[\frac{x_2 - x}{\sqrt{(x_2 - x)^2 + (a-y)^2 + z^2}} - \frac{x_1 - x}{\sqrt{(x_1 - x)^2 + (a-y)^2 + z^2}} \right] \quad (2.11)$$

Using the above analytical equations, the magnetic field generated by a wire segment which is placed on the Y-axis, and its variation along X-axis at a height $z = 150 \mu\text{m}$, carrying a current of $I = 0.2 \text{ A}$ was studied, and is as shown in fig. 2.4. The peak intensity of the magnetic field is 0.251mT (B_x) at the center of the wire. The intensity of B_z is highest at either side of the wire, about 0.142mT and their signs are opposite to each other

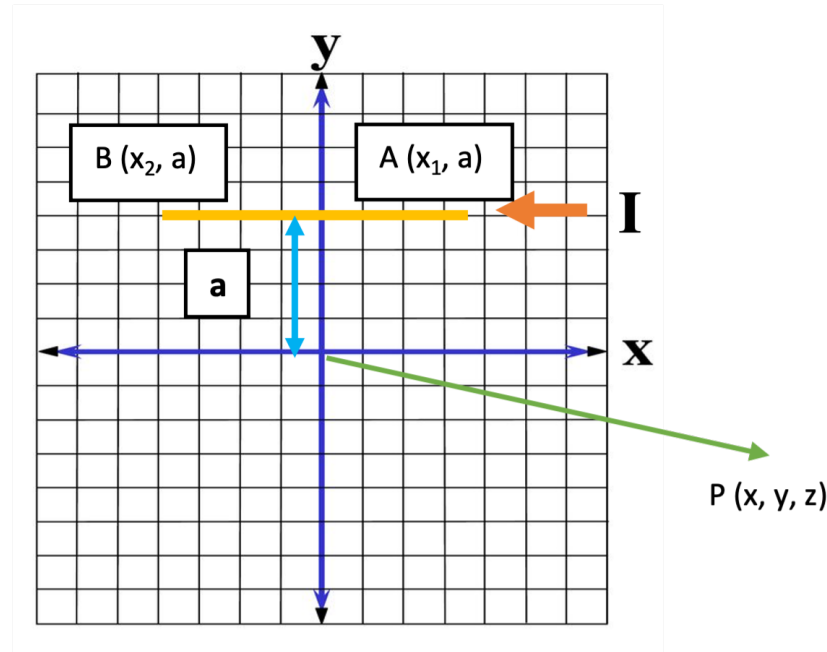


Figure 2.3: Conductor carrying current I , placed at a distance ‘ a ’ from origin parallel to X-axis on X-Y Plane

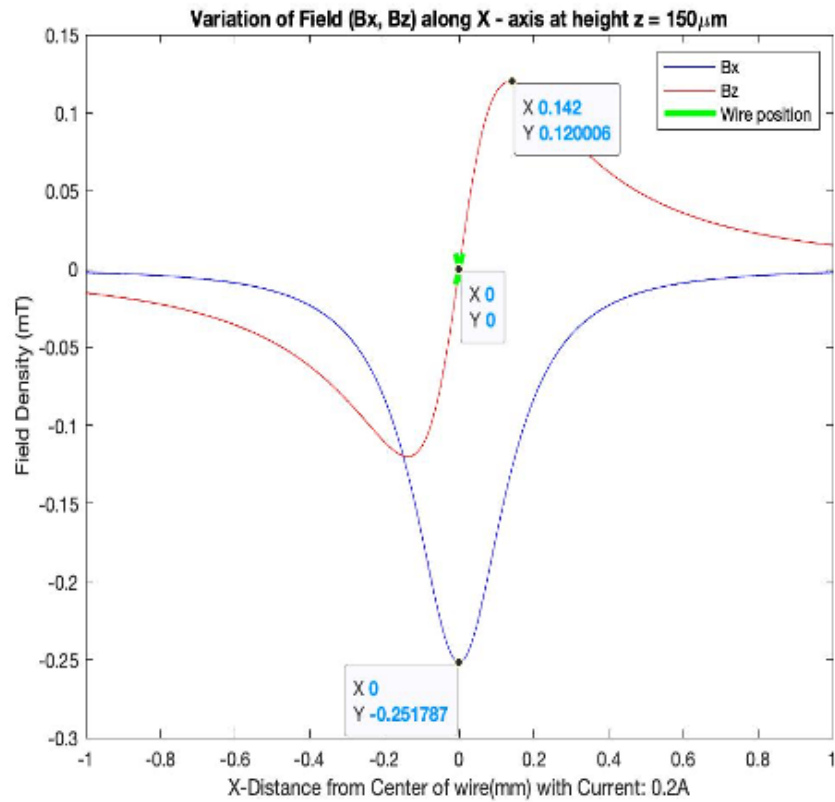


Figure 2.4: Analytical Result of Variation in Field (wire is into the plane)

The results obtained from the analytical formulae were compared with a FEM model based on COMSOL, where a strip of wire which is 254 μm wide, 1000 μm long and 35 μm thick carrying 0.2 A along the length of wire is considered and the field data at a height of $z = 150 \mu\text{m}$ was obtained and shown in Fig 2.5. The values obtained were similar to analytical solutions.

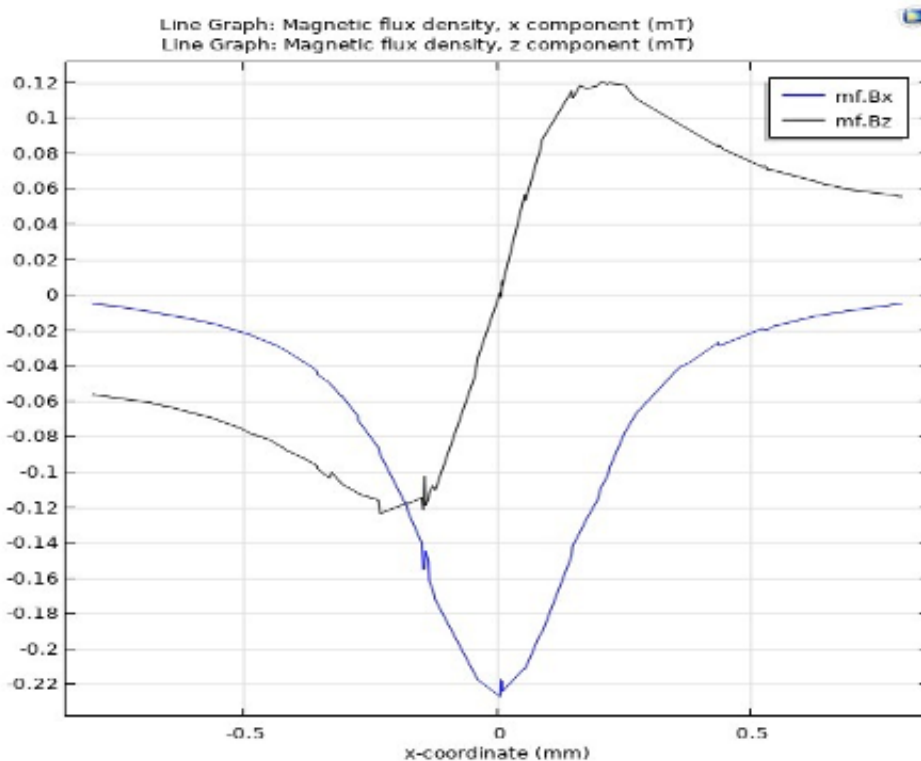


Figure 2.5: FEM Model Based variation of Magnetic Flux Density on COMSOL

2.2.2 Gradient of Magnetic field of a straight wire segment with finite length

The magnetic field gradients in a workspace which are directly proportional to magnetic forces can be determined using the analytical solutions. The gradients can be seen in Fig 6, the intensity of dB_x/dx and dB_x/dZ have field gradient intensities of $\approx 1.8 \text{ T/m}$ at center of the wire and $\approx 1 \text{ T/m}$ on either side of wire respectively.

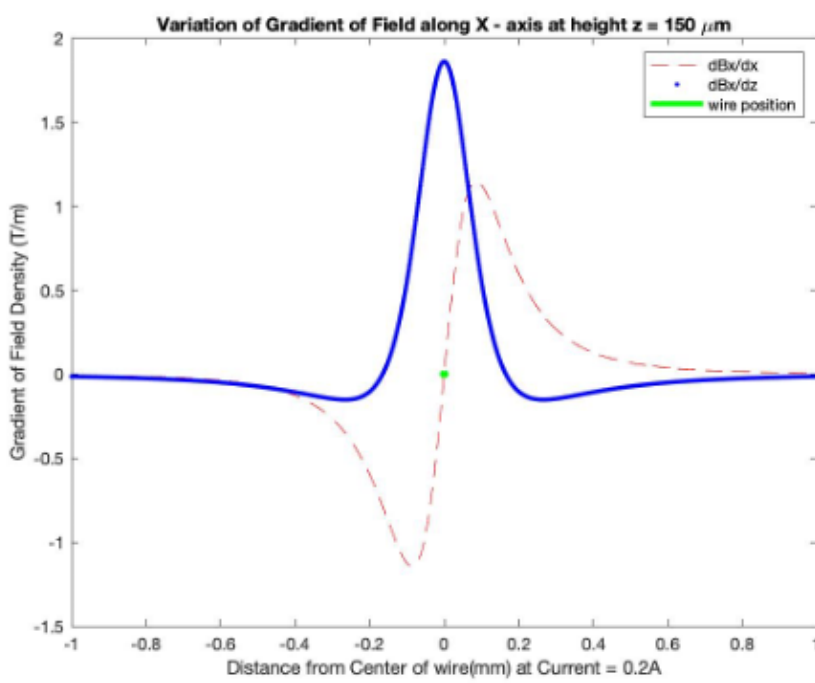


Figure 2.6: Variation of Gradient of Field (B_x) along X axis at height $z = 150 \mu\text{m}$

2.2.3 Magnetic force generated by straight wire segment with finite length on the micro bot

Considering, a N35 cylindrical magnet of diameter 2mm and thickness 0.9 mm with a magnetic flux density of 1.45 T, it can be assumed without loss of generality that the robots have higher magnetization (M_z) along Z-axis (out of the plane) and the current-carrying wire is placed parallel to Y axis, this results in $B_y = 0$, hence zero magnetic gradients associated with B_y . The magnetic force acting on bot is now reduced to equation as shown below as $M_z \gg M_x, M_y$

$$F_{mag} \approx \nu M_z \left(\frac{dB_x}{dz} \hat{i} + \frac{dB_z}{dz} \hat{k} \right) \quad (2.12)$$

The magnetic force along the X-axis when the magnetization is aligned in the Z-axis is shown in Fig 2.7. It can be seen that the magnetic force acting on the bot is greater than the frictional force, hence now the bot can be either attracted or repelled based on how the poles of the bots are placed.

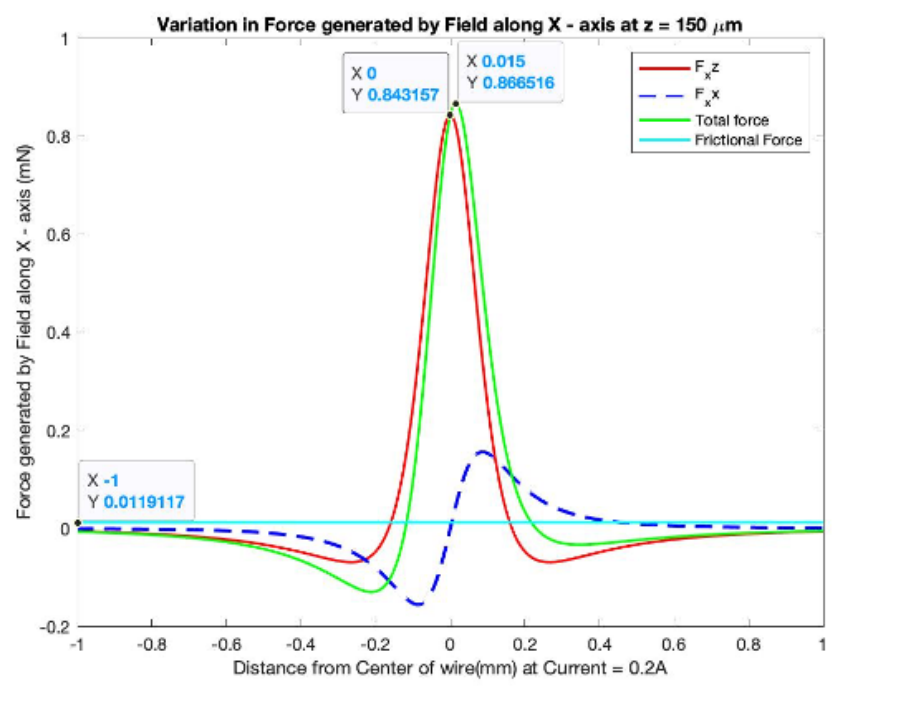


Figure 2.7: Variation of Gradient of Field (B_x) along X axis at height $z = 150 \mu\text{m}$

The force equation now contains both x – component and z – component, hence it is possible for the bot to move along the plane [if $F_{mag, x} > F_{mag, z}$] or get toppled out of the plane [if $F_{mag, z} > F_{mag, x}$ and $F_{mag, z} > mg$, (where m is the mass of the bot and g is the acceleration due to gravity)], as shown in fig 2.8. Hence, to control the motion of the bot along the 2D plane, we need to always ensure that $F_{mag, x} > F_{mag, z}$. and $mg > F_{mag, z}$, as shown in fig 2.9.

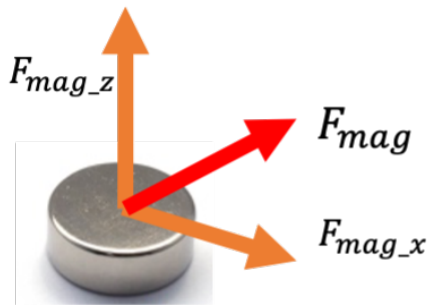


Figure 2.8: Magnetic forces acting on the cylindrical bot

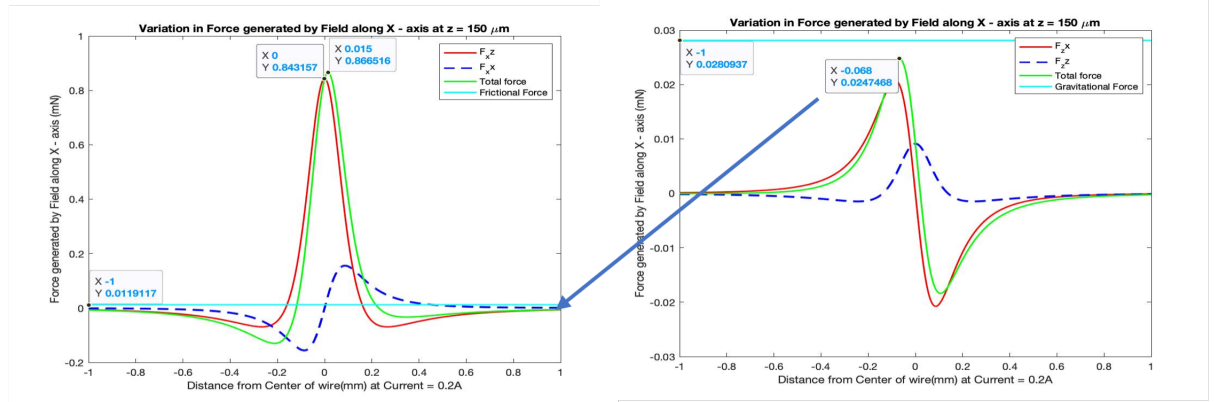


Figure 2.9: Comparison of $F_{mag, x}$ and $F_{mag, z}$

It can be seen from the above image that the Gravitational force acting on the bot is higher than the $F_{mag, z}$, and the peak intensity of $F_{mag, z} \approx 0.025$ mN which is comparatively very low than the peak intensity of $F_{mag, x} \approx 0.87$ mN.

2.2.4 Magnetic Field due to a rectangular coil

The above results shows us that the microbot can be moved even with a single strip of wire along the 2D plane, but now comes the part where how should these strips of wire (traces) be placed on the PCB, so that maximum range of magnetic forces can be generated to control the micro bot's movement of any size. Getting a higher range of force implies a higher range of control of micro bot's movement. The types of traces can be

1. Single-segment wires places parallel to each other in a rectangular array
2. Single segments wires connected to each other forming a polygon and these polygons are placed in the form of an array
3. Using Serpentine coils of PCB

The types of traces that can be made on the PCB, are shown in fig 2.10.

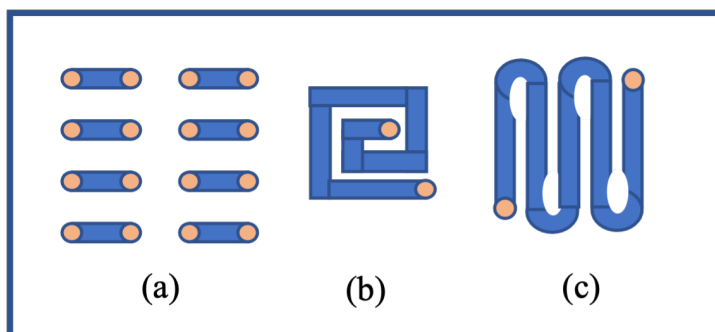


Figure 2.10: Different types of traces on PCB

The Biot – Savart's Law follows the principle of superposition, i.e., the total field due to multiple current-carrying segments acting on a point is the summation of individual field acting on that given point. The magnetic flux density of the planar coils can be determined by superposition of the field vectors of all the wire segments, and it's components are given by

$$B_{x, \text{coil}} = \sum_{i=1}^n B_{x,i} \quad (2.13)$$

$$B_{y, \text{coil}} = \sum_{i=1}^n B_{y,i} \quad (2.14)$$

$$B_{z, \text{coil}} = \sum_{i=1}^n B_{z,i} \quad (2.15)$$

, where i is the segment number.

As there are 3 types of traces on PCB, possible it is desirable to find which kind of design will have high range of force and has a higher range of influence on bot's movement (i.e., the maximum distance till which a particular segment can generate enough force to overcome frictional forces acting on the microbot). To identify which trace is more suitable, four parameters were considered, which effect the force acting on the microbot, they are:

1. Magnitude of Current
2. Increasing the no. of turns (i.e., increasing no. of connections between the wire segments
3. Increasing the layers of PCB
4. Height at which the bot can be placed.

2.2.5 Variation of Force acting on the micro bot

2.2.5.1 Changing the current in the coils

The field generated by the coils depends on the current's magnitude and direction, and as the field is directly related to force, the current passing through coils is also directly related to the amount of force applied on the microbot. Hence by increasing the magnitude of current, we can get an higher range of force, which can be controlled by controlling the amount of current sent through the coils. Below image shows the variation of force for different magnitudes of current in case of permanent magnet.

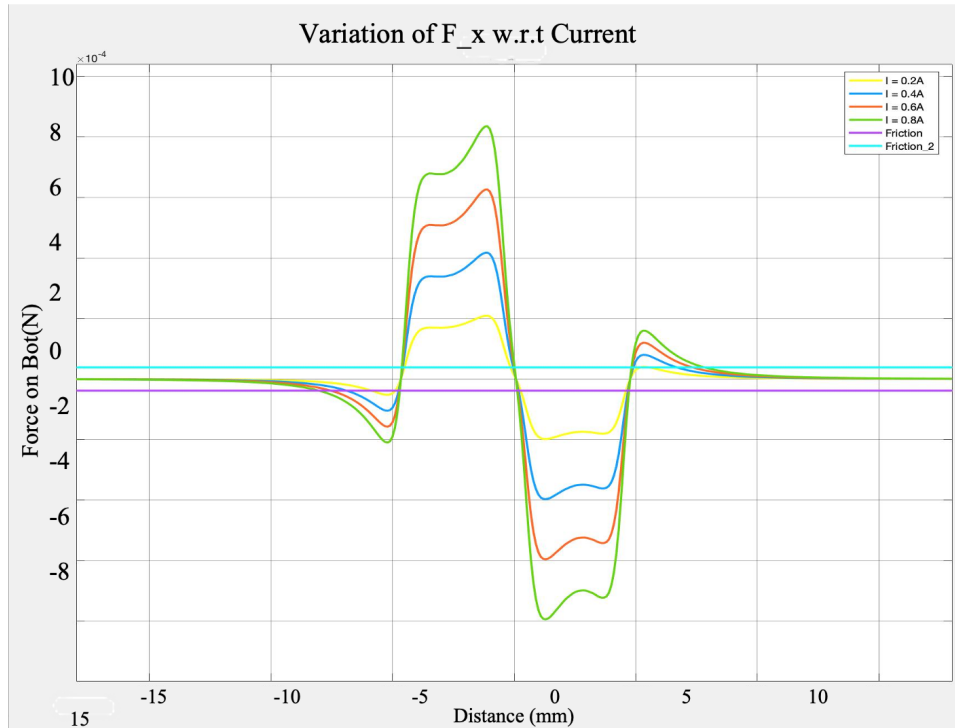


Figure 2.11: Analytical Result of Variation of Force on bot w.r.t Current

When an ferromagnet is considered, there Magnetization(M) is proportional to flux density (B), hence Force will be proportional to I^2 . Table 2.2 shows where we numerically observe the changes in range of force with respect to change in current through the coils.

Current(A)	Peak-Peak Magnitude (mN)	%Improvement	Influencing Distance (mm)	%Improvement
0.2	0.407		10.58	
0.4	0.814	100	10.48	-0.9
0.6	1.222	199.75	10.36	-2.07
0.8	1.63	300.49	10.14	-4.15

Table 2.2: Change in range of force with respect to change in current through the coils

The major issue with increasing the current is that, as these coils are made of copper, each coil has an associated resistance with it that depends on the length of coil and the area of cross-section of the coil, hence as the magnitude of current increases, the power dissipated in the form of heat will also increase significantly making PCB hot and the permanent magnet (NdFeB) is also a good conductor of heat, because of this the inherent magnetism of the magnet reduces, hence it is not a good option to just increase the current. Also, if we increase the current, the range of influence for a given coil decreases as the slope of magnitude curves increase at the location where both magnetic force line and frictional force line intersect, implying that the

segment cannot generate enough force to overcome friction which can be seen in the table 2.2. Hence increasing only current is not a feasible option.

2.2.5.2 Increasing no. of turns in the same plane

It is intuitive that as the no. of turns in the same plane increases the range of influencing distance of force on the bot also increases. Not only does the influencing distance increases, but also it is observed that the range of magnitude of force acting on the microbot also increases significantly, although not as proportionate as compared to increase in the current. The variation of force acting on the bot for different no. of turns in the same plane can be seen figure 2.12

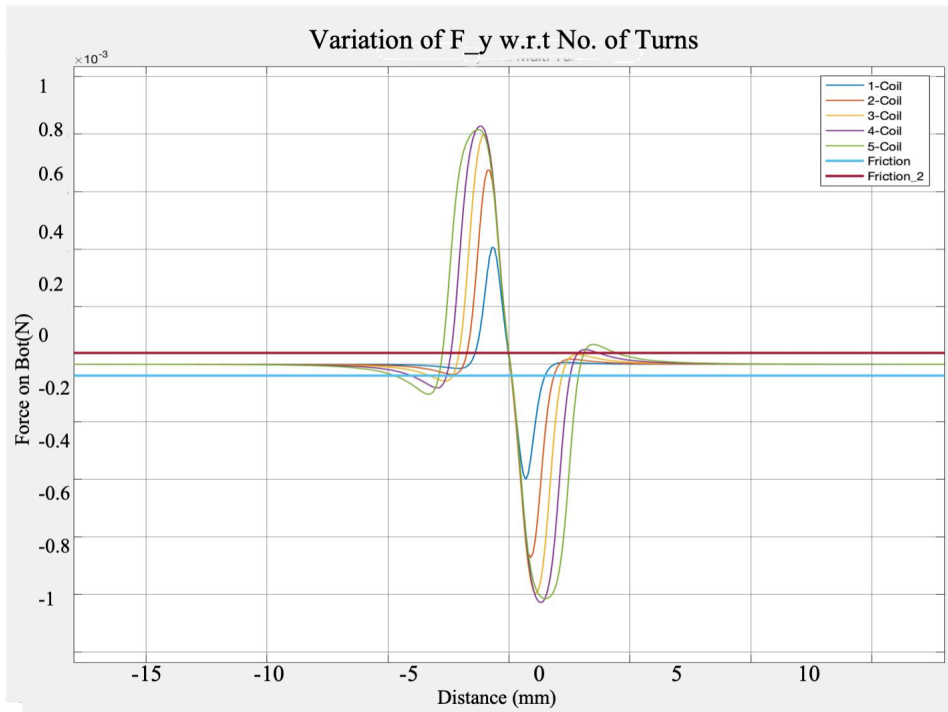


Figure 2.12: Analytical Result of Variation of Force on bot w.r.t No. of Turns for $I = 0.7A$

The table 2.3 shows how both range of force and influencing distance is dependent on the no. of turns.

No. of Turns	Peak Magnitude (mN)	%Improvement	Influencing Distance (mm)	%Improvement
1	-4.064		4	
2	-6.747	66.01	4.8	20
3	-7.982	96.40	6.1	52.5
4	-8.277	103.66	7.8	95
5	-8.146	100.44	9.3	132.5

Table 2.3: range of force and influencing distance vs the no.of turns

From table 2.3, it can be observed that increasing the no. of turns in the same plane is better.

2.2.5.3 Increasing no. of turns in the same plane

In PCB, there is an option to increase the no. of layers of the board, and these layers are interconnected to each other using ‘vias’. For a current of 0.7A as the number of layers of the PCB board increases, it can be seen from the figure below that both the range of force and influencing distance is increasing.

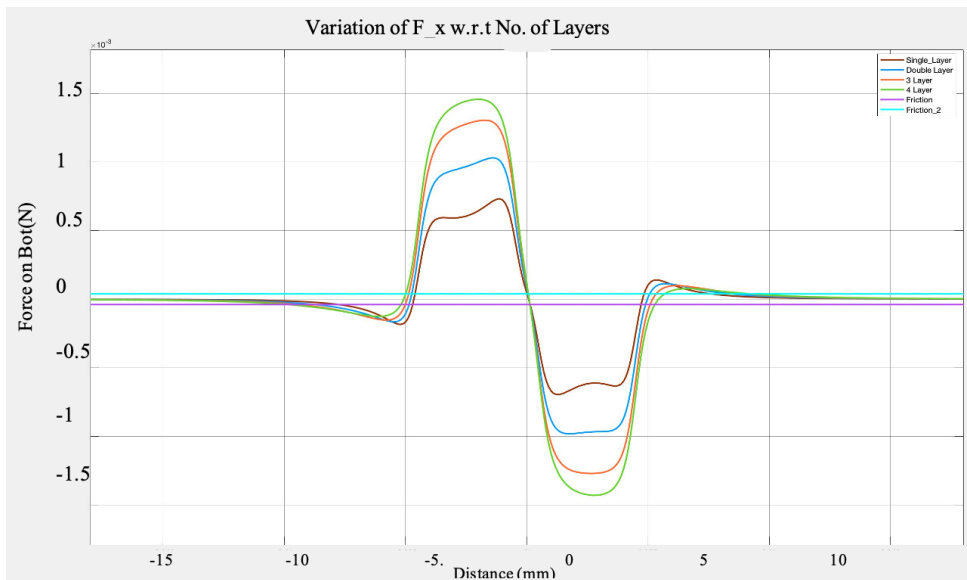


Figure 2.13: Analytical Result of Variation of Force on bot w.r.t No. of Layers of PCB, for $I = 0.7\text{A}$

The variation results can also be seen numerically in the table 2.4, where it can be observed that as the no. of layers increases, the range of force increases significantly.

No. of Layers	Peak-Peak Magnitude (mN)	%Improvement	Influencing Distance (mm)	%Improvement
1	1.426		15.4	
2	2.011	41.23	17.2	11.68
3	2.575	80.57	18.5	20.12
4	2.886	102.38	19.1	24.02

Table 2.4: No. of layers increases vs the range of force increases

2.2.5.4 Height from PCB

Magnetic forces for a single segment of wire along the plane has a range of 0.4mm (refer Fig. 2.9). It shows that the range at which the bot’s motion can be controlled is in order of

micrometres. A similar attempt was made to study the distance at which the bot can be placed over the PCB and can be still controlled. From the below image it can be observed that when the current sent through the wire segment is 0.7A magnitude of force increases till $700 \mu\text{m}$, but later as we go away from PCB, the force acting on the bot decreases rapidly, proving that the coils should be very close to the microbot to get higher range of force.

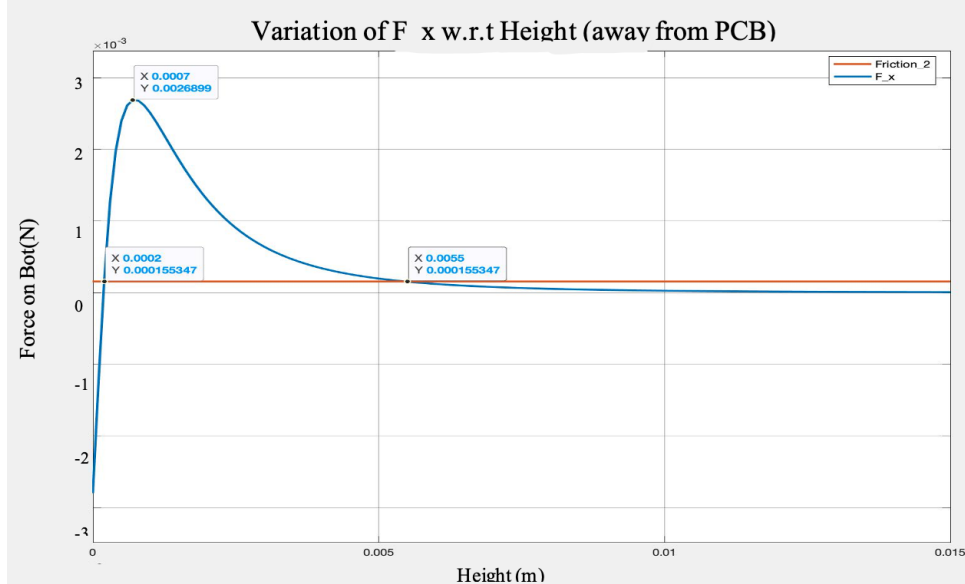


Figure 2.14: Analytical Result of Variation of Force on bot w.r.t Height away from PCB for $I = 0.7\text{A}$

2.2.6 Design Choice of Coil on PCB

Based on the above analysis of variation of force with respect to current, no. of layers, no. of turns and height away from PCB, to get the higher range of magnetic force and range of influencing distance, it is desirable to design a multi-turn segment of wires connected to each other and distributed across in an array and to have a multi-layer PCB board. Note that the coil should have higher current carrying capacity implies that the resistance of the coil should be as low as possible and the microbot can either be directly placed on the PCB, or at a height $< 1\text{mm}$ away from the PCB to avoid thermal conduction of the magnets.

2.2.7 Comparison of Forces acting on the type of material of the micro robot

As discussed earlier, the type of material of the micro robot can either be a permanent magnet or a ferromagnet. In the application of localized control, where multiple robots can be controlled independently, for Ferro magnets there would not be any interacting forces among the micro-robots, therefore they can be placed as close as possible and still be controlled independently unlike a permanent magnet where the microbots get influenced by each other's field. Permanent magnets either attract each other such that it is difficult to separate them or repel each other such

that it is difficult to join the multiple micro robots. Eventhough from the above explanation, it seems plausible that using a ferromagnet is more beneficial than using a permanent magnet, but because of the inherent magnetic field present in the permanent magnets, it is possible to move them due to their higher magnetization, as can be seen in the image below that the force acting on permanent magnet for $I = 0.7\text{A}$ is in order of mN. As ferromagnets depend on the magnitude of the external field for their magnetization (see equation 2.4), the force generated by the coils for $I = 0.7\text{ A}$ is in order of μN , which is far less than the frictional force acting on the ferromagnet and hence the ferromagnet will not even move in the 2D plane. Below image shows the comparison of forces acting on different type of materials of the micro robot.

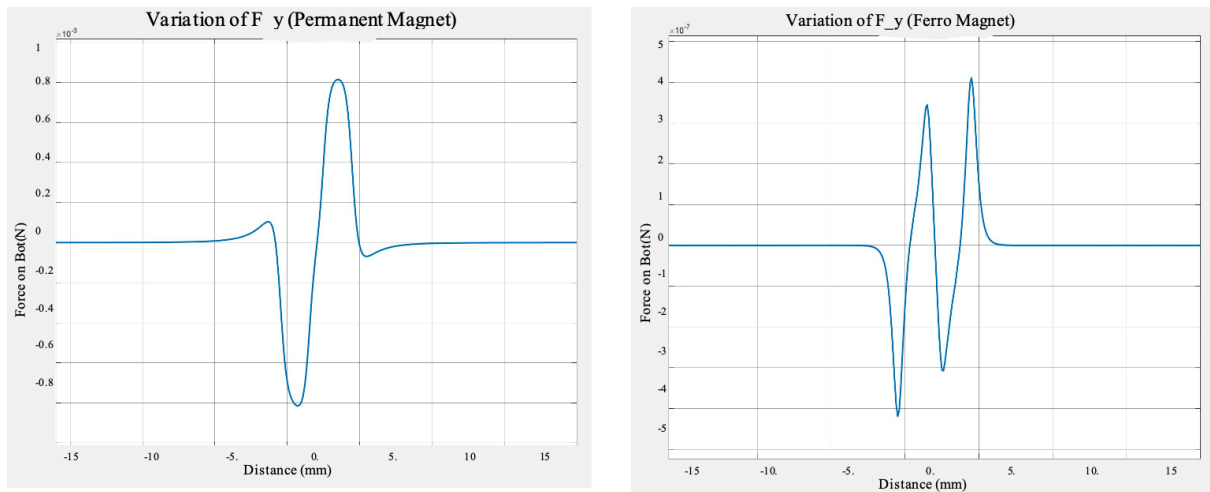


Figure 2.15: Comparison of Analytical Result of Variation of Force on bot w.r.t type of material $I = 0.7\text{A}$,

a) Permanent Magnet b) Ferro Magnet

2.2.8 Final PCB Design

From the above analysis it can be noted that using an array of multi turn coils on a multi layered board is the better option, hence the design in Figure 2.16 was made on Ki CAD 6.0 having following specifications mentioned in the table 4.2.

PCB Specifications	
No. of Coils	64 (8x8 array)
No. of Layers	2-4
PCB Thickness	1-2mm
Coil Specifications	
No. Turns in Coil	8-10
Trace Width	0.25mm
Spacing between traces	0.15mm
Trace Thickness	0.035mm
Maximum Current Carrying Capacity (for $\Delta T=20^\circ\text{C}$)	1.2A
Maximum Coil side length	9.8mm
Resistance of Coils	0.7 – 1 Ohms
Inductance of Coils	2.5 μH

Table 2.5: PCB and Coil Specifications

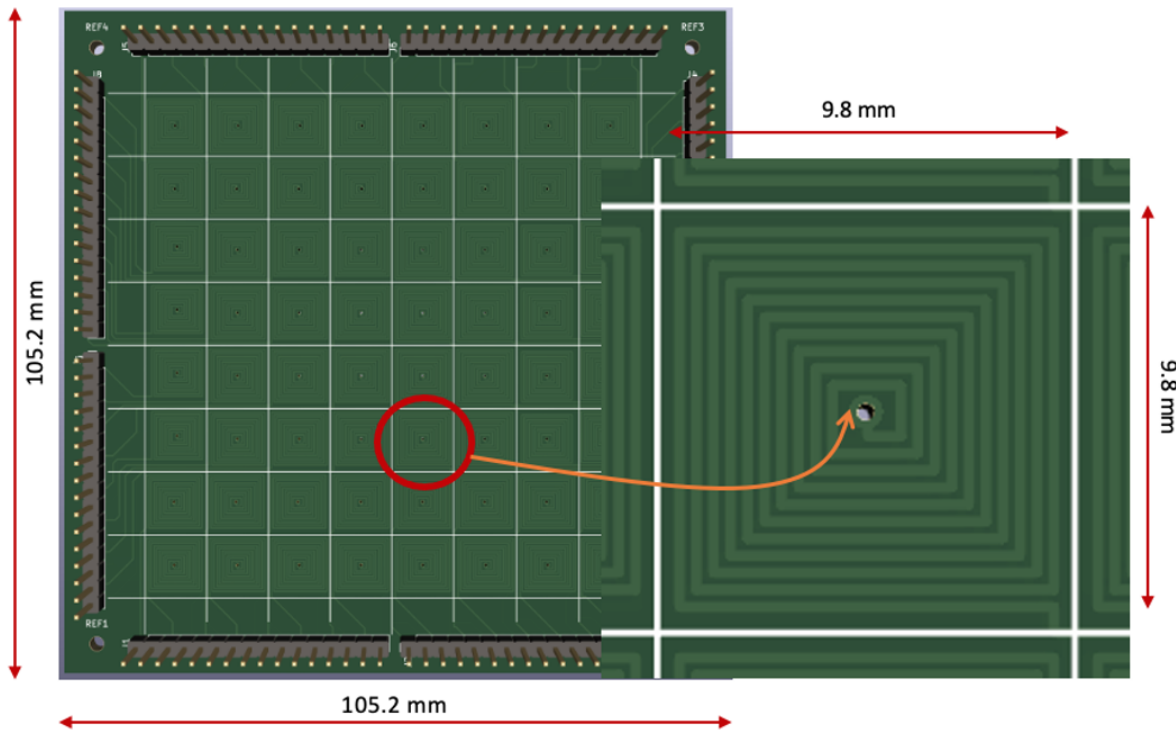


Figure 2.16: PCB Design

2.2.9 Losses in the Designed coil

The current sent through the coil must be from a PWM voltage source as we need a variable current source to turn on multiple coils at the same time. The coils have an inherent resistance that dissipates energy from heat. The resistance (R) of coils ranges from 0.7 – 1 Ohms, hence

the maximum power loss (I^2R) due to resistance of the coil for a current (I) of 0.7A is 0.49W per coil. The PWM voltage sources operate at a certain frequency and the permanent magnet NdFeB is a conductor of electricity, hence when it is placed in varying magnetic field eddy currents are produced in the magnet, whose value can be found out using the equation below,

$$P_e = K_e * f^2 * B_{max}^2 * t^2 \quad (2.16)$$

, where K_e is the eddy current constant given by Volume of the bot divided by Resistivity of Copper. At $f = 50\text{Hz}$, for $I = 0.7 \text{ A}$, B_{max} of coil is 23 Gauss and t is the thickness of the bot which is equal to 0.9mm, the losses due to eddy current is found out to be 4.3nW. Hence the maximum loss produced by the system are resistive losses.

2.3 Experimental Verification

The above discussions and results obtained were based on the analytical solutions, to ensure that the system is behaving as like the analytical solutions, the field generated by the designed coil was measured using a Digital Gauss meter from SES Instruments. When readings were measured, the sensor was attached to a precision meter by Butter Instruments and was hovered on the coil. Later the measurements obtained were compared with the analytical solutions and the error at the center of coil was around 1.2 %, but as we go far away from center of the coil the margin of error was increased till 33%, when the sensor was placed 8mm away from center of the coil (outside the coil).

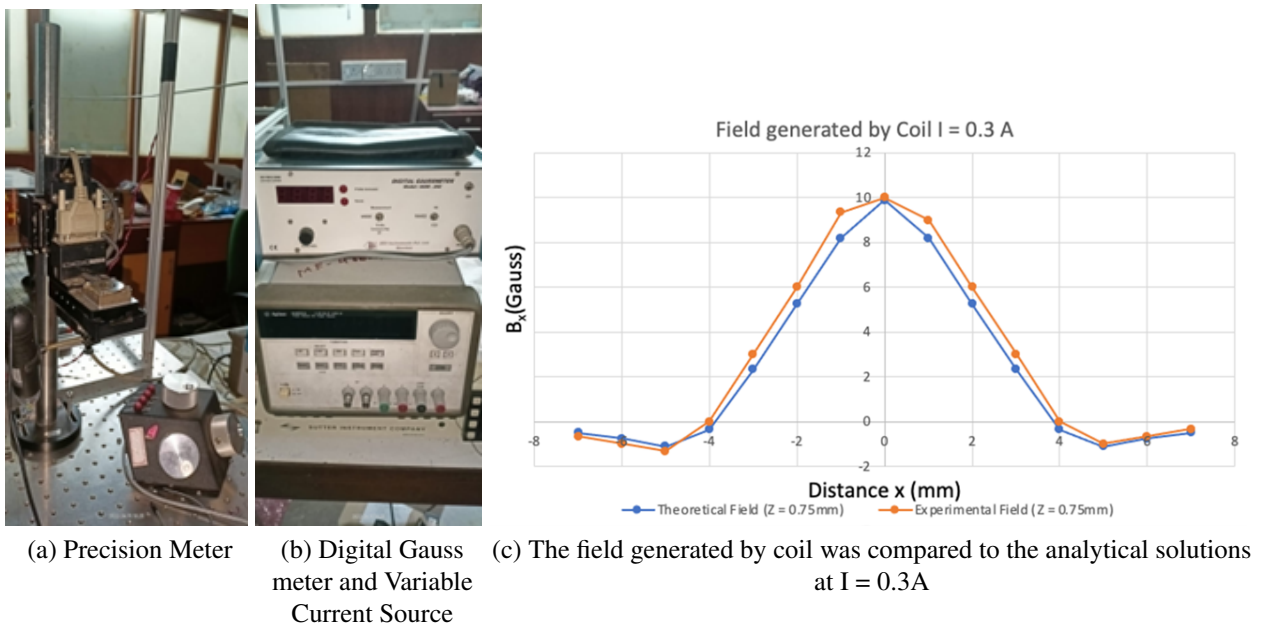


Figure 2.17: Experimental setup for field measurement

Later a Simulink model was also made on Simscape, MATLAB to understand the dynamics of the system. The Simulink model was done based on the analytical equations as discussed

earlier and can be seen in the image below. In the simulations it was observed that when both coil and the microbot are attracting each other, the microbot always comes to the center of the coil and oscillates at center, but when the coil and the microbot repel each other, the motion of the microbot is not predictable as it depends on both the magnitude of the current and the position where the bot is placed on the coil. For a given value of current, even a small change in the position of the bot (in few μm) it was observed that bot's movement was not predictable when both coil and the microbot repel each other. Hence there is a requirement to control the motion of the bot, to move the bot is a desired trajectory.

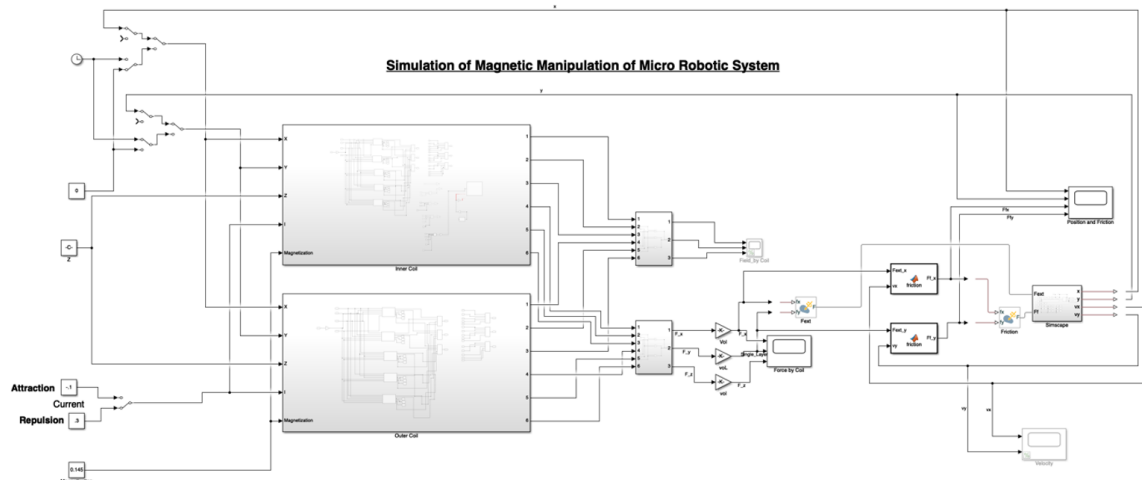
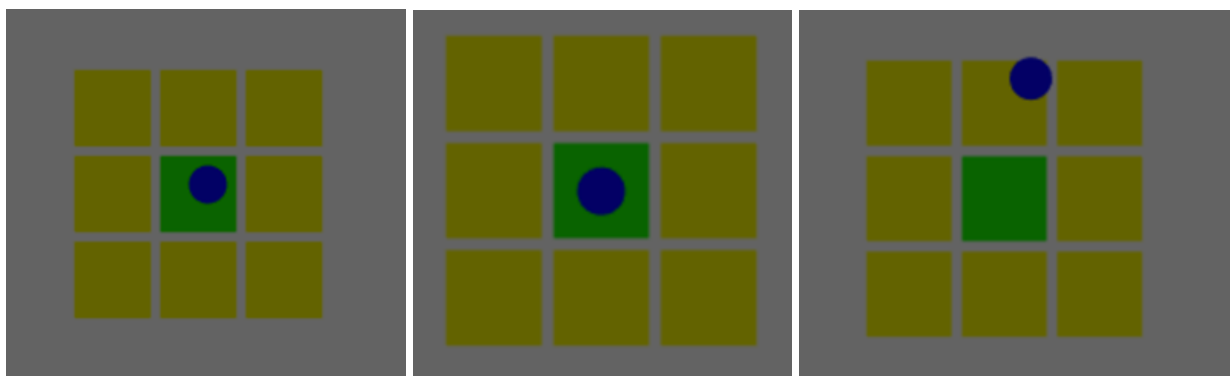


Figure 2.18: Simulink model replicating the dynamics of the system



(a) Initial Position of the bot (Blue) placed on the coil (Green) (b) Final position when bot and the coil are attracted to each other (c) Final position when bot and the coil are repelling each other

Figure 2.19: Robot repulsion and attraction in Simulink model

Chapter 3

EXPERIMENTAL TEST-BED DESIGN

This chapter describes the components used in the experimental test bed in Section 3.1 and their inter-connections, forming a system, in Section 3.2. Experimental test-bed core components consist of printed PCB, electronics for current control through coils, a camera feedback system, a computer for processing, and a controller for sending signals to the electronics.

3.1 COMPONENTS

3.1.1 PCB

The printed circuit board(PCB) coils, in the shape of square spirals, were designed in KiCAD 6.0 and were ordered from PowerPCB. The PCB design work is described in detail in the dissertation submission by S Surya Teja.

Figure 3.1 shows a zoomed view of a single coil, and the following are the Coil Design Specifications.

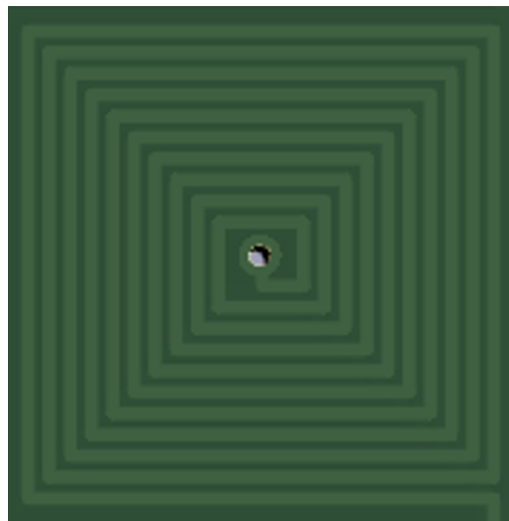


Figure 3.1: Zoomed in view of a single coil

1. No. of Turns = 8-10
2. Trace Width = 0.25mm
3. Spacing between traces = 0.15 mm
4. trace Thickness = 0.035mm
5. Max Current Carrying Capacity = 1.2A for $\Delta T = 20 \text{ } ^\circ\text{C}$
6. Max Coil side length = 9.8 mm
7. Resistance of coils = 0.7-1 Ohm
8. Inductance of coils = $2.5 \mu\text{H}$

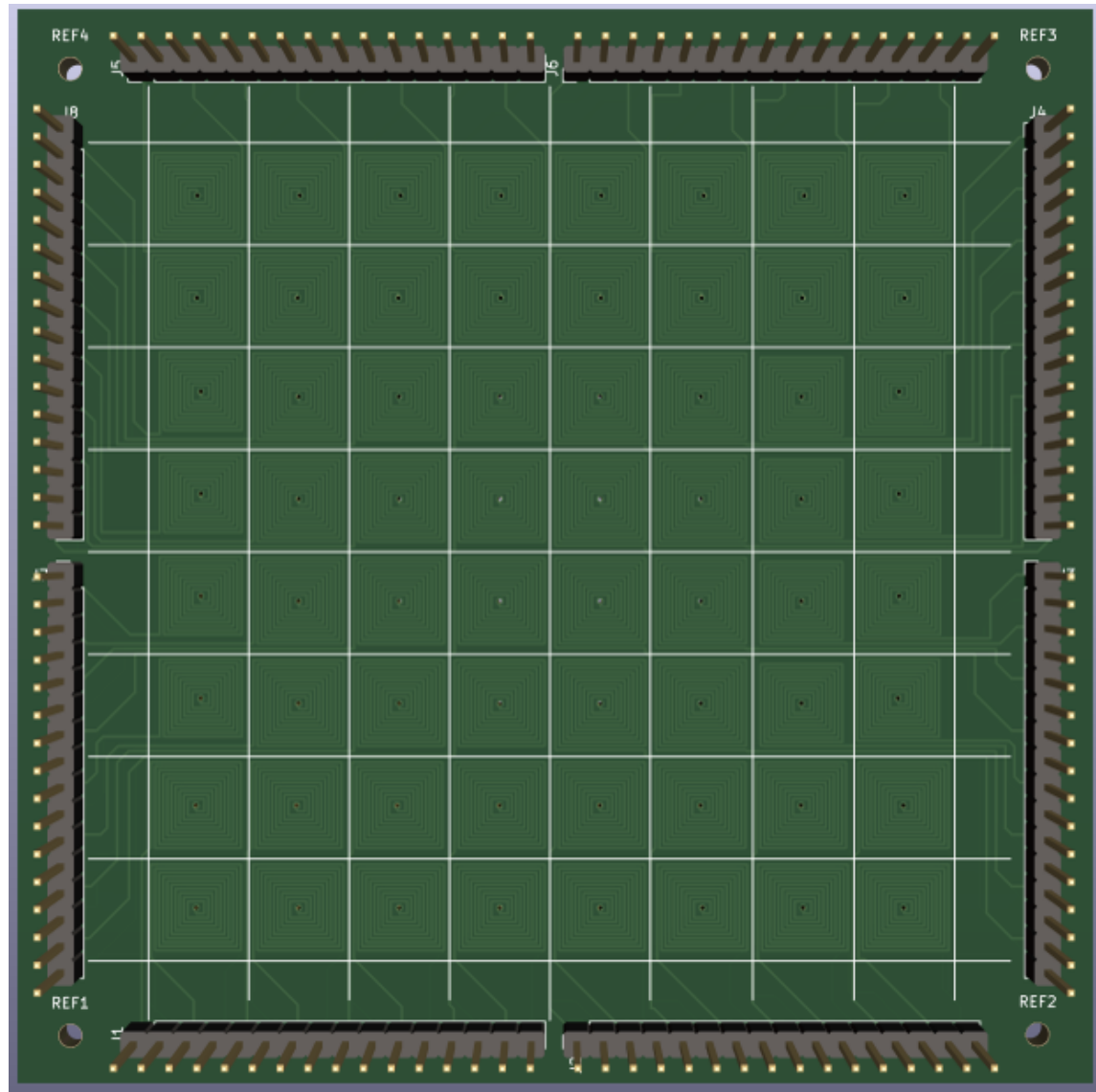


Figure 3.2: Final PCB Design with an 8×8 grid of spiral coils

Figure 3.2 on page no 24 shows the final design and following are the PCB specifications

1. Number of coils = 64
2. PCB layers = 2-4
3. PCB thickness = 0.6 mm

3.1.2 Robot

1. Material of the Micro Robot- The micro robot is actuated using an external magnetic field. Hence the robot that is chosen as a Permanent Magnet.
2. Shape of the Robot- The micro-robot can be of different shapes. Still, due to the manufacturing and control constraints, we have chosen a cylindrical micro-robot that is easy to maneuver on a 2D platform.
3. The dimensions of the Micro Robot are as follows:
 - Height of Bot = 0.9 mm
 - Radius of Bot = 2 mm
 - Volume of Bot = $\pi \times r^2 \times h = 11.31 \text{ mm}^3$
 - Density of Permanent Magnet = 7500 kg/m^3 (Considering NdFeB)

Figure 3.3 shows one of the permanent magnet cylindrical robots used



Figure 3.3: Permanent magnet robot and its dimensions

3.1.3 Electronics

To control the current through a coil on the PCB, a power circuit and a control circuit are required. For current control, MX1919 ICs are used. PCA 9685 and Arduino are used for PWM switching and direction control of current through the coil.

3.1.4 Voltage Control Driver IC- MX1919

This MX1919 Based Driver Module is a high-power driver used for driving DC Motors and Stepper Motors. It can control up to 2 outputs with directional and speed control. It can go up to 2.5A of current.

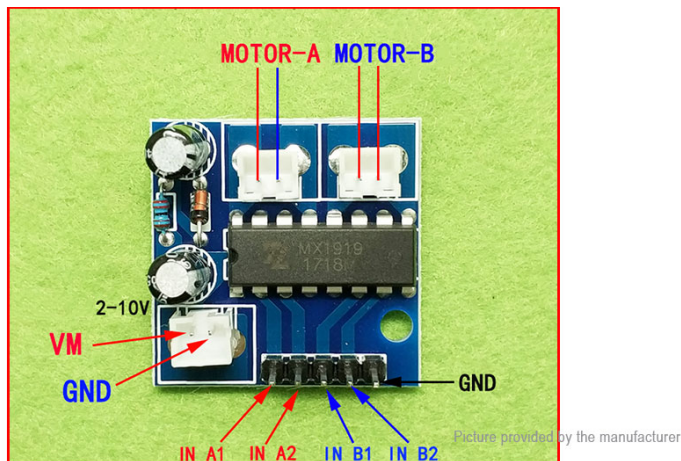


Figure 3.4: MX1919 Based Motor Driver Module – 2.5A

3.1.4.1 Pin Diagram

1. MOTOR-A: Motor A output
2. MOTOR-B: Motor B output
3. IN A1: 1st input for Motor A
4. IN A2: 2nd input for Motor A
5. IN B1: 1st input for Motor B
6. IN B2: 2nd input for Motor B

3.1.4.2 Technical Specifications

1. Module supply voltage: DC 2V-10V
2. Signal input voltage: DC 1.8-7V
3. Single working current: 1.5A
4. Peak current up to 2.5A
5. Low standby current (less than 0.1uA)
6. Built-in common conduction circuit, the input terminal vacant, the motor does not malfunction

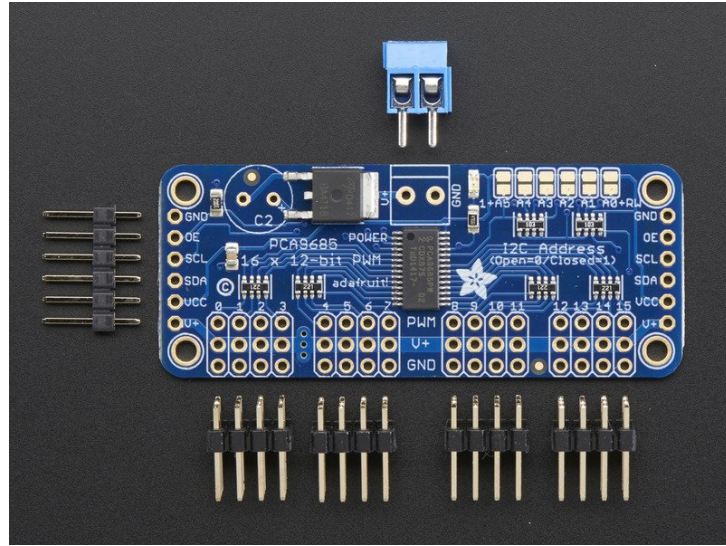


Figure 3.5: Adafruit 16- channel 12-bit PWM Driver

3.1.5 PWM Driver IC- PCA 9685

The Adafruit 16-Channel 12-bit PWM/Servo Driver will drive up to 16 servos over I2C with only two pins. The on-board PWM controller will operate all 16 channels simultaneously with no additional Arduino processing overhead. Moreover, it can chain up to 62 of them to control up to 992 servos with the same two pins!

The Adafruit PWM/Servo Driver is the perfect solution for any project that requires many servos.

3.1.5.1 Pin Diagram

1. SCL- I2C clock pin
2. SDA- I2C data pin
3. OE - Output enable. It can be used to disable all outputs quickly.
4. VCC - Logic power pin
5. GND - Power and signal ground pin
6. OUTPUT PORTS - There are 16 output ports. Each port has three pins: V+, GND, and the PWM output. Each PWM runs entirely independently.

3.1.5.2 Library reference commands

1. `setPWMFreq(freq)` : This function can be used to adjust the PWM frequency(40 Hz to 1600Hz).

2. setPWM(channel, on, off) : This function sets the start (on) and end (off) of the high segment of the PWM pulse on a specific channel. On/Off Range- 0 to 4095.

- channel: The channel that should be updated with the new values (0..15)
- on: The tick (between 0..4095) when the signal should transition from low to high
- off:the tick (between 0..4095) when the signal should transition from high to low

3.1.6 Power Supply

SMPS is used to power the MX1919 and, in turn, drive current through the coils. It had the following specifications

1. Input Voltage- AC 100-120 volt or 200-240 volt
2. Output Voltage- DC 5V, Output Current- 60A
3. Power- 300W
4. DC Switching Mode Power Supply

3.1.7 Camera

A camera is used to acquire feedback on the system, i.e., the bot's position in the workspace. The camera is mounted on the PCB, and the computer reads the acquired image for image processing.

The camera used is Logitech C270 Digital HD Webcam and has the following Technical Specifications.

1. Max Resolution: 720p
2. Image Capture Speed: 30 fps
3. Camera megapixel: 0.9
4. Focus type: fixed focus
5. Diagonal field of view (dFoV): 55°

Note- Image processing applications generally use more specialized high resolution and high FPS cameras. However general-purpose webcam also solved the purpose here. hence used

3.1.8 Controller

Arduino UNO R3 communicates with MX1919 driver ICs through the PCA9685 PWM driver. I2C pins on the Analog input side, A4 and A5, are connected to SDA and SCL pins on the PCA9685 PWM driver

3.2 CONNECTION OF COMPONENTS

Figure 3.6 shows a simplified circuit for a single MX1919 driver.

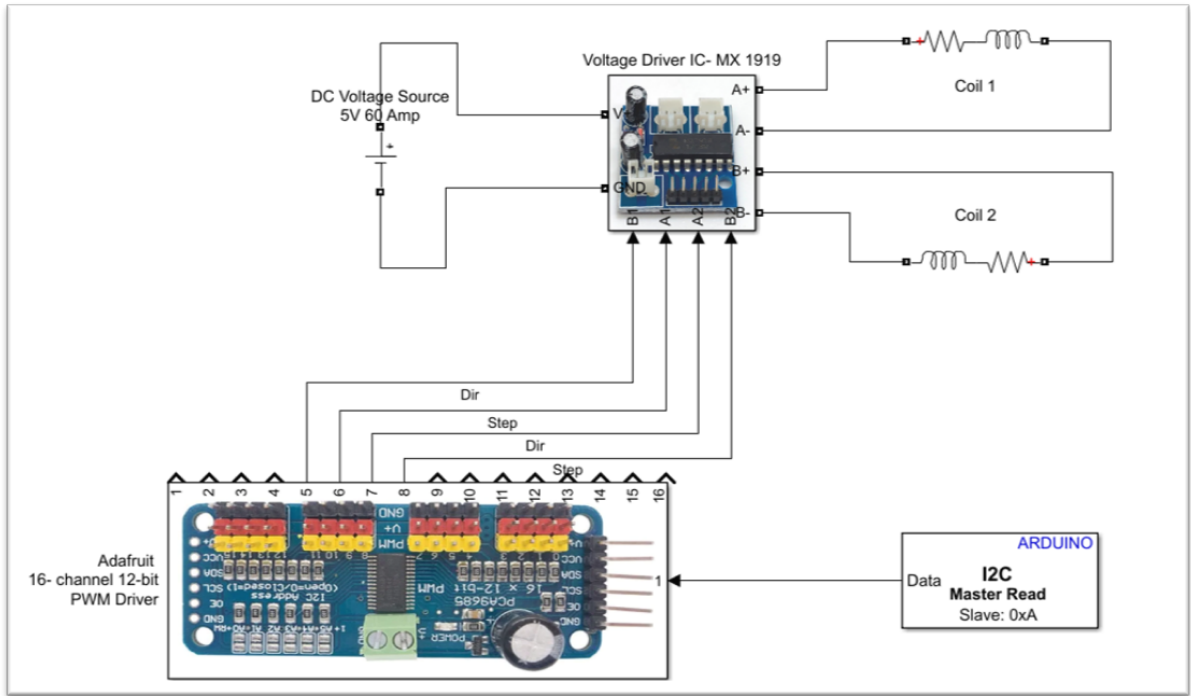


Figure 3.6: Simplified Setup Schematic

As discussed in section 3.1.4, each MX1919 driver IC can control current through 2 coils. Since, PCB has $8 \times 8 = 64$ total coils. So, 32 MX1919 voltage driver ICs are used.

Current magnitude and direction in each coil are controlled using step and direction pins. For 64 coils, separate step and direction pins are addressed. So using the PCA9685 drivers, a total of 128 pins (64 coils, 2 pins(direction and step) per coil) are addressed uniquely. Here, 8 PWM9685 Drivers are used, connected in sequence. They are controlled using I2C addressing.

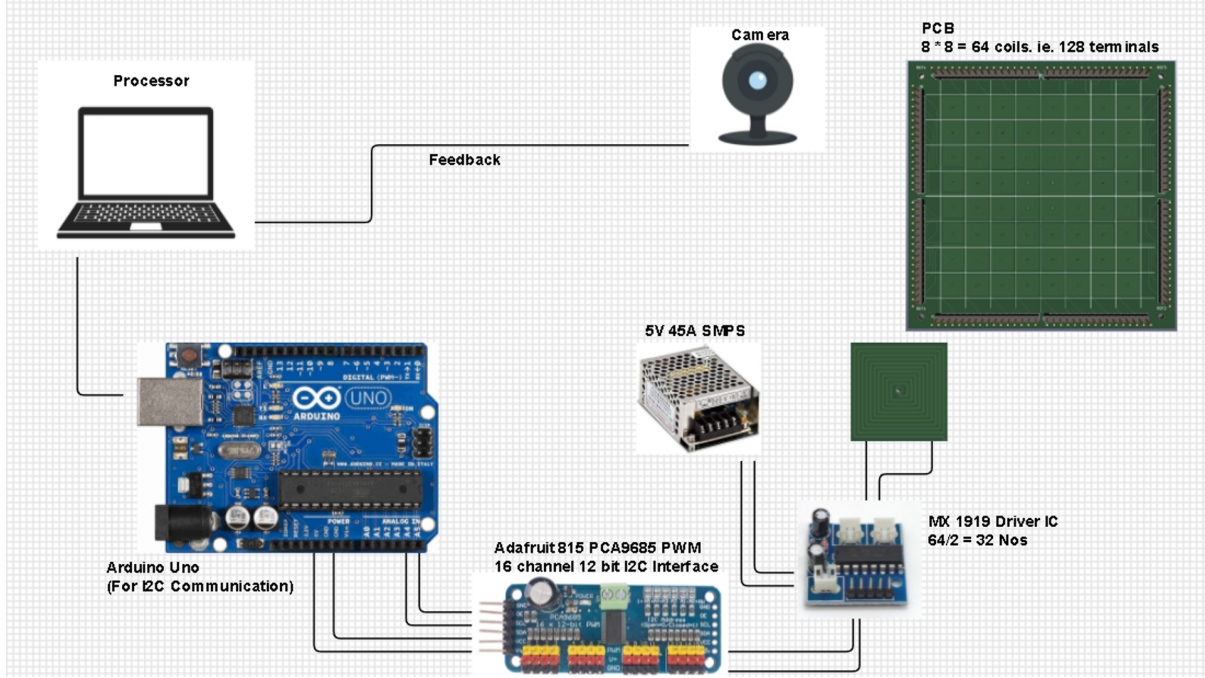


Figure 3.7: Setup Schematic with Camera Feedback

Figure 3.7 shows Camera feedback circuit. A camera mounted on the PCB captures the image and sends it to the processor. The image is processed using various computer vision techniques. The processor also decides on an individual coil or coils to activate/deactivate. Once, decision is made, regarding which coils to turn ON/OFF, the information is sent serially to Arduino, and Arduino sends it further to PCA9685 drivers using I2C communication.

The robots are placed with their north pole facing out of the plane of the PCB, with the top surface colored for easy tracking.

3.3 PICTURE OF FINAL SETUP

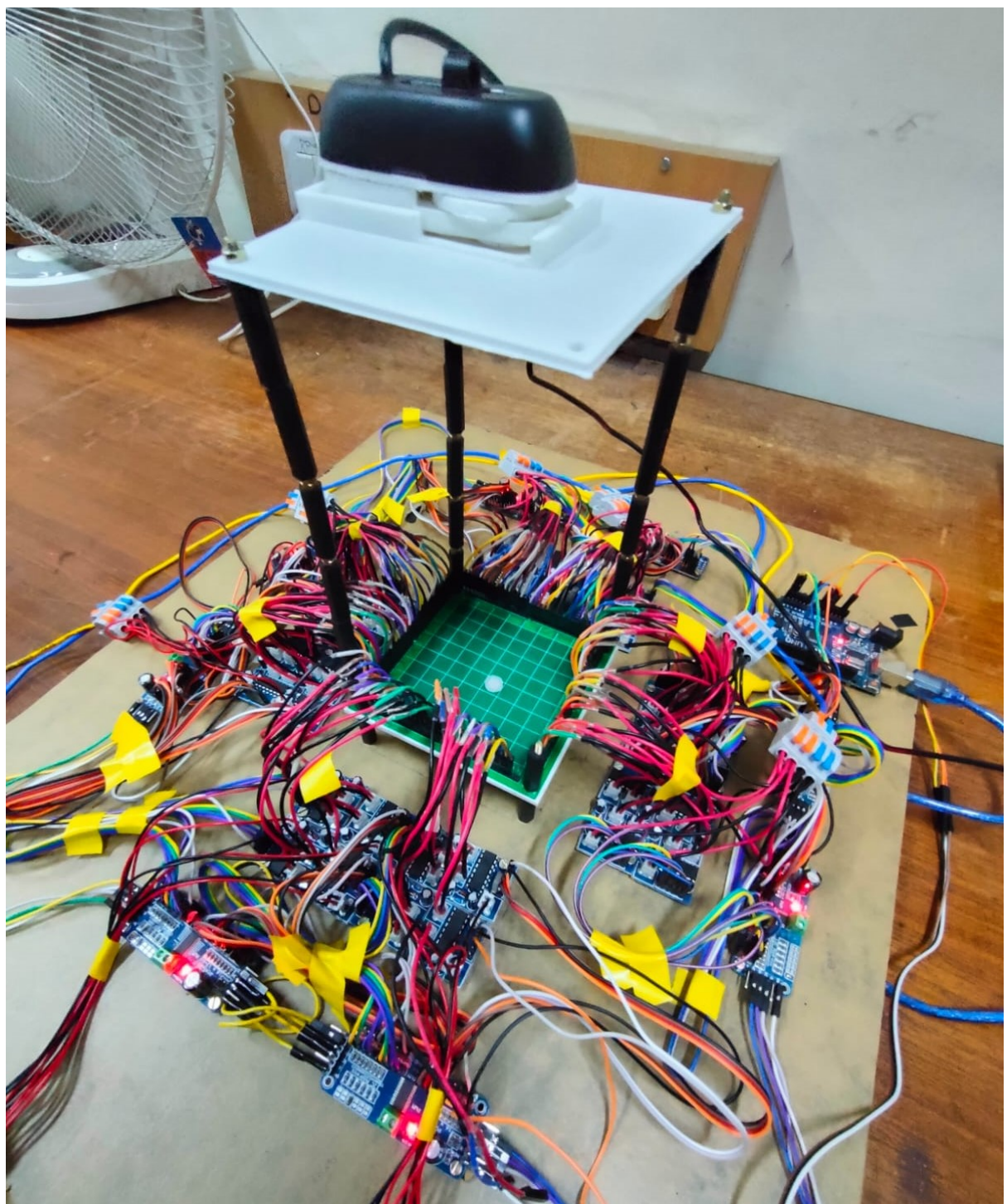


Figure 3.8: Final System

Chapter 4

IMAGE PROCESSING

Camera feedback is fed to the computer frame by frame for processing the image to calculate the robot's position and decide the actions required for future movement.

Digital image processing technique OpenCV is used to extract necessary information from the frame.

4.1 OpenCV - An Open Source Computer Vision Library

[18] OpenCV (Open Source Computer Vision Library) is an open-source computer vision and machine learning software library. OpenCV is built to provide a common infrastructure for computer vision applications and to accelerate the use of machine perception in commercial products.

In this implementation, we have used OpenCV in the python programming language in Linux 5.18.3 Operating system.

4.1.1 Identifying the edges of the coil array

The area captured by the image outside the coil array is discarded. This step ensures that only the robot's working area, i.e., coil array area, is processed, and unexpected information that may be read by the image outside the robot's working area is discarded. See figure 5.5 on 44

Program is written to identify four corners of the working area.

The output of the program is as follows.

Code 4.1: Output of get_new_references.py

```
1 edges = [[ 187,  76], # [Top Left x, Top Left y]
2           [ 173, 873], # [Bottom Left x, Bottom Left y]
3           [1001, 887], # [Bottom Right x, Bottom Right y]
4           [1002,  66]] # [Top Right x, Top Right y]
```

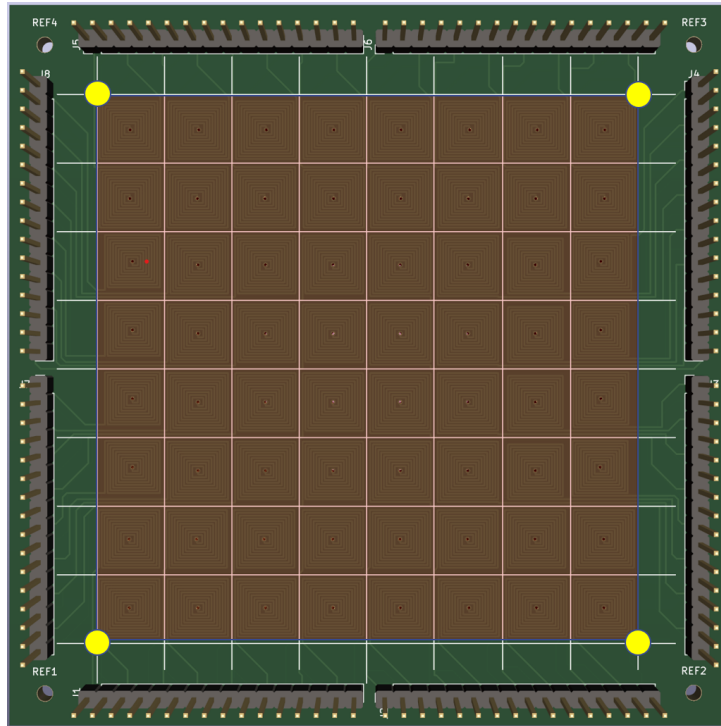


Figure 4.1: Figure shows 4 corners of the working area with Yellow circles and working area is highlighted in Red

4.1.2 Image Preprocessing

The 640×480 pixels frame is resized to 1280×960 pixels to get a bigger image and precise coordinates. Edges of the PCB coils are identified, and the portion outside the PCB coils is masked to get only the workspace image, as shown in the figure. The BGR image is further converted to grayscale. Also, blurring and erosion are used to diminish the noise and small features on the image.

Code 4.2: Code snippet for preprocessing

```

1 # Capture the video frame by frame
2 (_, frame) = vid.read()
3 # Frame resize
4 frame = cv2.resize(frame, (1280, 960), fx=0, fy=0, interpolation=cv2.
   ↪ INTER_CUBIC)
5 # Masking image inside workspace
6 mask = np.zeros(frame.shape[0:2], dtype=np.uint8)
7 points = np.array([edges]) # [edges] -> array containing PCB coil
   ↪ edge pixel coordinates
8 cv2.drawContours(mask, [points], -1, (255, 255, 255), -1, cv2.
   ↪ LINE_AA)
9 frame = cv2.bitwise_and(frame, frame, mask = mask)
10 # Use the cvtColor() function to grayscale the image
11 gray = cv2.cvtColor(frame, cv2.COLOR_BGR2GRAY)
12 # Used to diminish the noise and small features in the image

```

```

13 kernel = np.ones((5,5), np.uint8)
14 gray_blurred = cv2.medianBlur(gray, 11)
15 eroded=cv2.erode(gray_blurred,kernel,1)

```

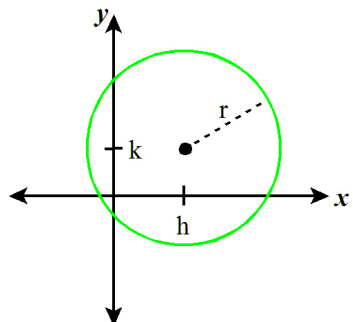
4.1.3 Identifying robots location

Once an image is acquired, identifying the exact location of the robot is essential. As discussed in the previous section, we use a cylindrical permanent magnet of a radius of 2mm to 4mm. The Center of the robot is considered the robot's location.

To identify the Center we use, (1) Hough Transform and (2) Finding points on the robot contour and averaging to get the Center

4.1.3.1 Hough Transform

[19] The Hough Transform is a method used in image processing to detect any shape if that shape can be represented in mathematical form. A circle can be described by the equation in figure 4.2 on 35:



$$(x - h)^2 + (y - k)^2 = r^2$$

Figure 4.2: Equation of circle

We may fix a point (x, y) to detect circles. We must find three parameters: h , k , and r . Therefore, the problem is in a 3-dimensional search space. The algorithm uses a 3-D matrix called the "Accumulator Matrix" to find possible circles to store potential a , b , and r values. The value of ' h ' may range from 1 to number of rows, ' k ' may range from 1 to number of columns, and r may range from 1 to $\text{maxRadius} = \sqrt{\text{rows}^2 + \text{cols}^2}$.

The HoughCircles function in OpenCV has the following parameters, which can be altered according to the image.

1. Detection Method: OpenCV has an advanced implementation, HOUGH_GRADIENT, which uses the gradient of the edges instead of filling up the entire 3D accumulator matrix, thereby speeding up the process.

2. dp: This is the ratio of the resolution of the original image to the accumulator matrix.
3. minDist: This parameter controls the minimum distance between detected circles.
4. Param1: Canny edge detection requires minVal and maxVal. Param1 is the higher threshold of the two. The second one is set as Param1/2.
5. Param2: This is the accumulator threshold for the candidate detected circles. By increasing this threshold value, we can ensure that only the best circles corresponding to larger accumulator values are returned.
6. minRadius: Minimum circle radius.
7. maxRadius: Maximum circle radius.

4.1.3.2 Finding points on the robot contour and averaging to get the Center

Contours are the line joining all the points along an image's boundary with the same intensity. OpenCV has a `findContour()` function that helps extract the contours from the image. Since the robot is a circle in the image, once the contour is identified, all contour points can be averaged to get the approximate Center of the robot.

4.2 Identifying coil centers and corners

Once the robot's position is known, it is crucial to understand the underlying coil below the robot. Centers of the coils and the corners, i.e., points of intersection of coils, are identified and stored in an array.

The 4 corners identified using `get_new_references.py` is used and remaining points are extrapolated. Also, the centers and corners are numbered for identification. The python code snippet stores [X, Y, Center/Corner number]. The figure 4.3 on page no. 38 shows a snippet of work-area identifying center and corner waypoints.

Code 4.3: Storing center/corner waypoints pixel co-ordinate and Center/Corner number

```

1 # Array declaration for center and corner waypoints
2 corners = np.zeros([9, 9, 3], dtype=int)
3 centers = np.zeros([8, 8, 3], dtype=int)
4
5 # Storing corners waypoints in the 'corners' array
6 for x in range(9):
7     corners[x][0][0] = round(edges[0][0] + x * ((edges[1][0] -
8         edges[0][0]) / 8))
8     corners[x][0][1] = round(edges[0][1] + x * ((edges[1][1] -
9         edges[0][1]) / 8))
9     corners[x][8][0] = round(edges[3][0] + x * ((edges[2][0] -
    edges[3][0]) / 8))

```

```

10    corners[x][8][1] = round(edges[3][1] + x $\times$ ((edges[2][1] -
11        ↪ edges[3][1]) / 8))
12    for y in range(1,8):
13        for x in range(9):
14            corners[x][y][0] = round(corners[x][0][0] + y $\times$ (
15                ↪ corners[x][8][0] - corners[x][0][0]) / 8))
16    corners[x][y][1] = round(corners[x][0][1] + y $\times$ (
17                ↪ corners[x][8][1] - corners[x][0][1]) / 8))
18
19    # Numbering corners waypoints and storing in the 'corners' array
20    i = 101
21    for x in range(1,8):
22        for y in range(1,9):
23            corners[x][y][2] = i
24            i = i + 1
25
26    # Storing center waypoints in the 'corners' array and numbering the
27    ↪ centers
28    i=1
29    for x in range(8):
30        for y in range(8):
31            centers[x][y][2] = i
32            centers[x][y][0] = round(corners[x][y][0] + (corners[x][y +
33                ↪ 1][0] - corners[x][y][0]) / 2)
34            centers[x][y][1] = round(corners[x][y][1] + (corners[x + 1][y
35                ↪ ][1] - corners[x][y][1]) / 2)
36            i=i+1

```

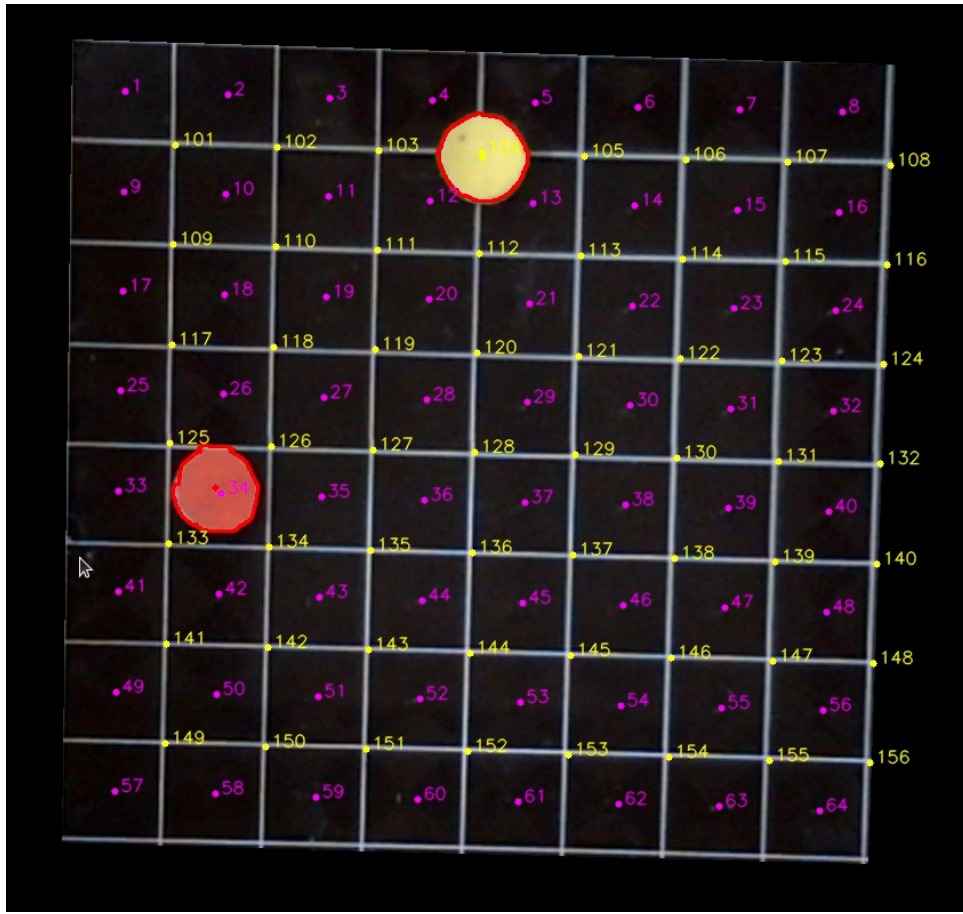


Figure 4.3: Center waypoints in yellow and Corner waypoints in pink

4.2.1 Colour Detection of robot

To distinguish a particular robot uniquely, the detection of the color of the robot is vital. The acquired BGR frame is converted to HSV color format using `cv2.cvtColor(frame, cv2.COLOR_BGR2HSV)`

Since, Hough transform/contouring-averaging technique gave the center of each robot identified. Finding the color of pixel of center of robot (`x_bot, y_bot`), helped differentiating the two robots In Open CV, BGR and HSV ranges used are

COLOR	BLUE	GREEN	RED	HUE	SATURATION	VALUE
RANGE	0-255	0-255	0-255	0-180	0-255	0-255

Table 4.1: BGR and HSV ranges used

Hue (h) color ranges were specified, for each colour. Table shows Differenet Colours annd their hue ranges used are

Color	Hue Lower	Hue Upper
RED	0	15
YELLOW	16	45
GREEN	46	75

Table 4.2: Hue ranges for different colors used

Chapter 5

ROBOT MOTION CONTROL

After modeling setup and image acquisition, this chapter focuses on the process employed to actuate the robot at any discretized location in the planar 2D coil array.

5.1 Local equilibrium point modeling

The currents in a spiral coil will either repel, forcing the robot to move outward, or attract and pull it towards its center, depending on the current's direction. The figure 5.2 on page no 42 shows the nature of the force generated along the X-axis of the coil at the height of 150 um and a current of 0.2 Amp. As can be seen from the nature of the graph, the Magnitude of force produced inside the coil, i.e., from -1 mm to 1 mm, is very high compared to outside the coil. Also, the force outside the coil is opposite to that inside the coil. So, When the robot has an attractive potential, this will attract the robot if it is inside the bounds of the coil. Meanwhile, if the robot is out of the bounds of the coil, the coil and robot will repel each other.[20]

Figure 5.1 (a) and (b) on page no 41 shows forces acting on the robot depending on the direction of the current and position of the robot

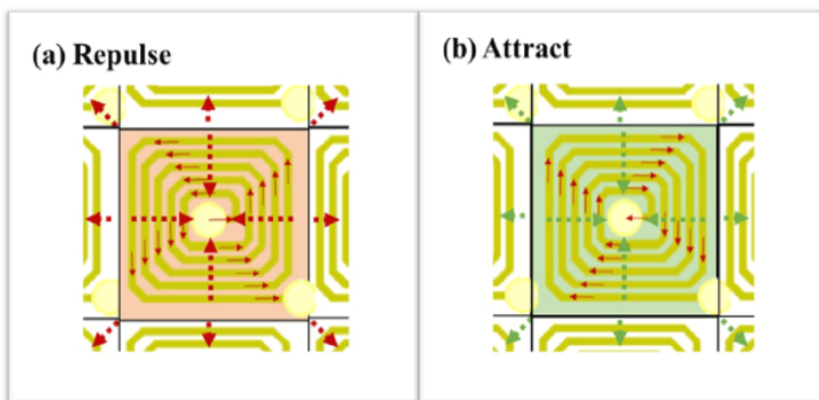


Figure 5.1: Forces acting on the robot depending on the direction of the current and position of robot

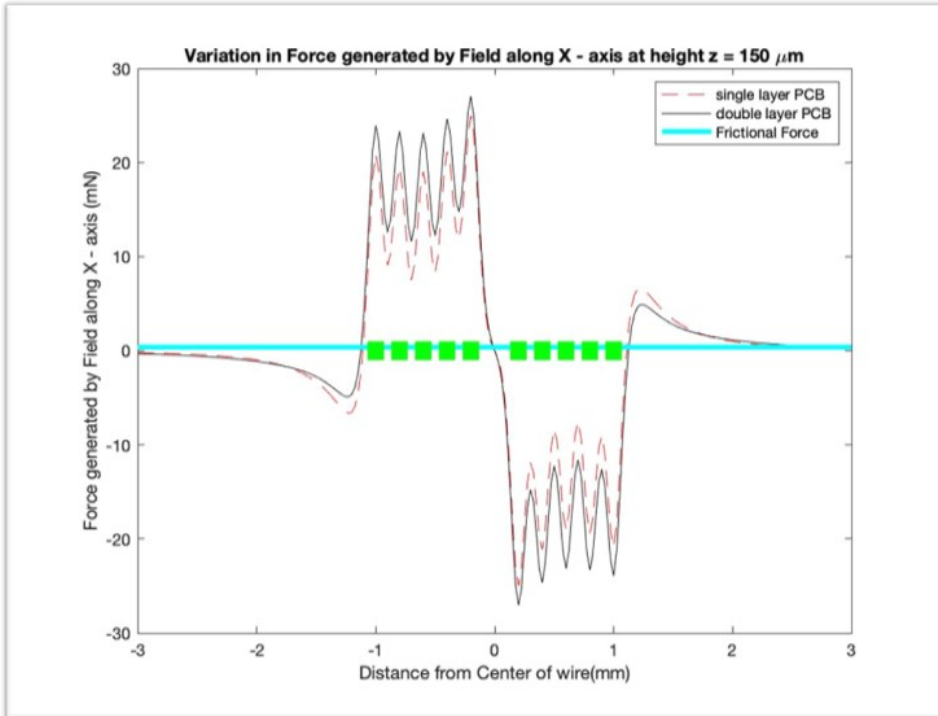


Figure 5.2: Overall Force generated by the coil along X-axis. Coil range -1 mm to 1 mm

Two points are identified as local equilibrium points, i.e., points of lowest magnetic potential. They are the centers of every coil and corner around the coils. So, as seen from figure 4.3 on page no 38 for the robot to move from one point to another on the workspace, it has to move alternately from a center to a corner and a corner to a center.

5.2 Types of possible movements

5.2.1 Corner to Center movement

To move a robot from a corner waypoint to a center waypoint, the center coil can be turned ON to attract the robot towards the center. Figure 5.3 shows the coil required to attract the robot from corner to center. Note- Green coil shows an Attractive field

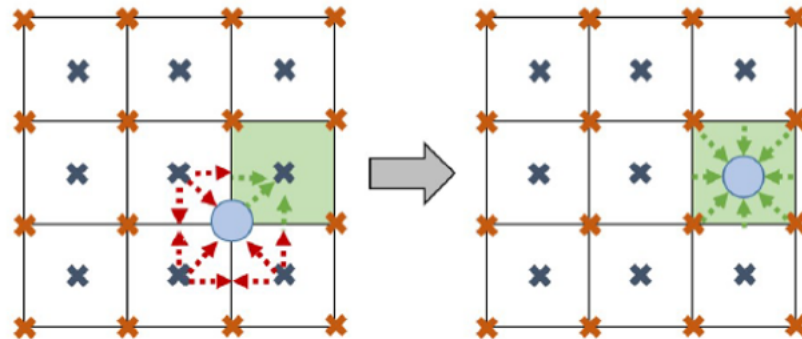


Figure 5.3: Coil required to attract the robot from corner to center, Green coil- Attractive field

Figure 5.4 shows coils turned ON initial and final states for center to corner movement. Here, one additional coil is also turned on in repulsive mode to assist the bot in its movement. Note, Red shaded coil is turned on as a Repulsive field, and the yellow shaded coil is turned on as an Attractive field.

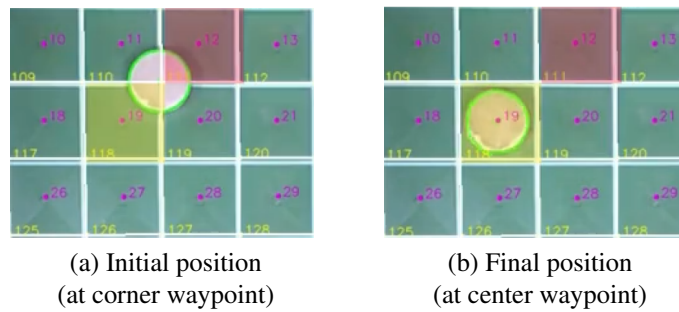


Figure 5.4: Corner to Center movement

Red shaded coil is turned on to repel the robot and yellow shaded coil is turned on to attract

5.2.2 Center to Corner movement

To move a robot from a center to a corner waypoint, A technique shown in figure 5.5 has to be employed. Since force exerted directly by turning the coil in repulsive mode when the robot is at the center generates a high magnitude of the force in the z-direction, throwing the robot away. So, the robot has to be moved towards the corner as shown in figure 5.5. Followed by pushing the robot to the corner by repealing all four coils. A two-step process is followed. Figure 5.5- Green coil shows an Attractive field, Red coil shows a Repulsive field.

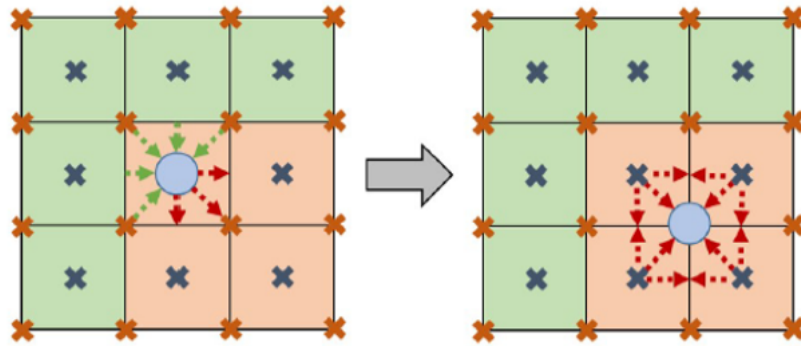


Figure 5.5: Coils required to attract the robot towards the corner.
Green coil- Attractive field, Red coil- Repulsive field

Figure 5.6 (a) shows initial position, where only 4 coils are turned ON (Yellow coils- Attractive mode and Red coils- Repulsive mode). Since adjacent coils produce maximum force. The remaining coils can be ignored practically. 5.6 (b) shows the intermediate position where the robot is moved away from the center(Aleast greater than five pixel) and towards the midway to the corner. Now, as shown in figure 5.6 (c), all four coils are turned into a repulsive mode to push the robot to the corner

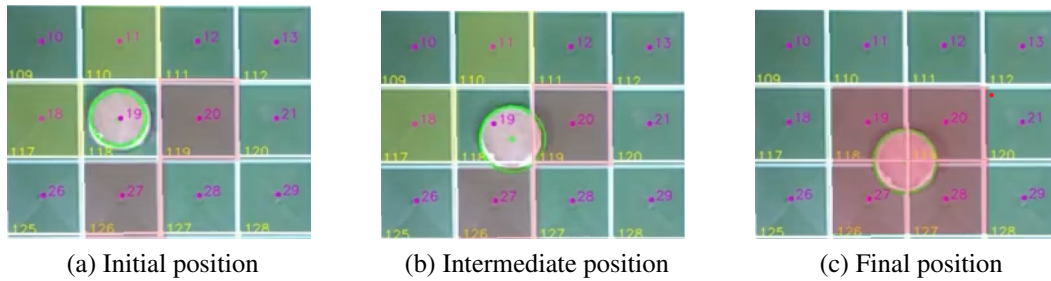


Figure 5.6: Center to Corner movement
Red shaded coil is turned on to repel and yellow shaded coil is turned on to attract

5.3 Path Planning

Finally, a path planning algorithm is required for the robot to decide its path to be traveled along with the board. Figure 5.7 shows an 8×8 coil array, the center and corner waypoints marked

with "x" are considered for developing path planning algorithm. Since, the map for solving has small number of points an grid based algorithm can be used. Grid-based approaches overlay a grid on configuration space and assume each configuration is identified with a grid point. At each grid point, the robot is allowed to move to adjacent grid points.

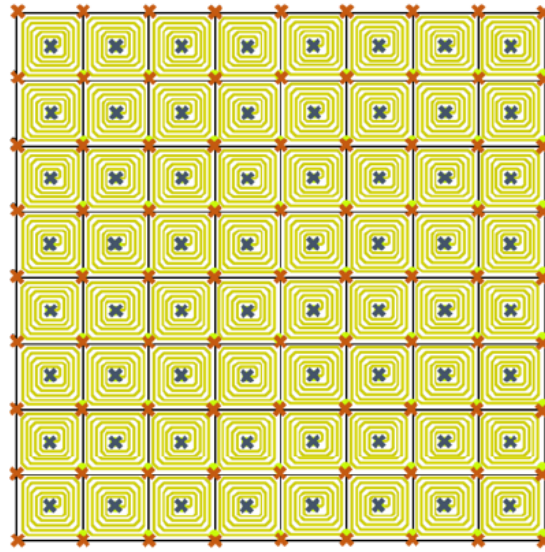


Figure 5.7: Waypoints for A^* algorithm consist of each coils center and corner positions, all marked with an "x".

A^* Algorithm has been implemented here, since it only finds the shortest path from a specified start to a specified goal. A typical A^* Algorithm has been deployed. Waypoints in figure 5.7 are fed as a array map to A^* Algorithm. Algorithm takes start configuration S from the camera depending on the robots position and goal configuration G is fed by the user. The path returned is used to identify series of coils to be turned ON to move the robot from start to goal. In cases where the robot strays from the defned path, this algorithm will be recomputed and bring the robot back to the desired waypoint.

Chapter 6

VALIDATION EXPERIMENTS

The first set of experiments conducted were to validate models presented in Section 5.3. A position based feedback is employed. The robots location obtained from camera is compared to stored array of coil center pixels and corner pixels(Refer Section 4.2). Based on the position of robot coils are actuated.

It was confirmed that the two motions- center-corner and corner-center with coil excitation are as discussed in 5.3. During corner-center movement, only one coil is excited, The motion is smooth, and the robot is attracted reliably. During center-corner movement, the Force required to move the robot from the center toward the corner is due to a set of surrounding coils turned ON in a specific manner. This Force acting on the robot is comparatively less. Also, It is important for position-based feedback that the robot is at least five pixels away from the center before starting the second step of the process. These two issues make corner point equilibrium more susceptible to errors caused due to uncertainties and disturbances in the workspace.

If the robot does not reach the local equilibrium point, the position-based control keeps the coils switched ON for longer. If the robot does not reach after a set timeout or moves to an undesirable place, the system is RESET. The robot is pulled back and tried again.

6.1 Single Robot Manoeuvring experiments

A single robot was tried to move from a random position to a specified GOAL position. The algorithm ran recursively until the GOAL state was reached. Figure 6.1 (a),(b),(c),(d),(e) shows intermediate positions as the robot moves from its START state at corner 129 to GOAL state at corner 111.

Figure 6.2 shows a single robot manoeuvring from START state 117 to GOAL state 15. The figure also shows the shortest path planned using A^* algorithm(In black) and the actual path taken by the robot(In red)

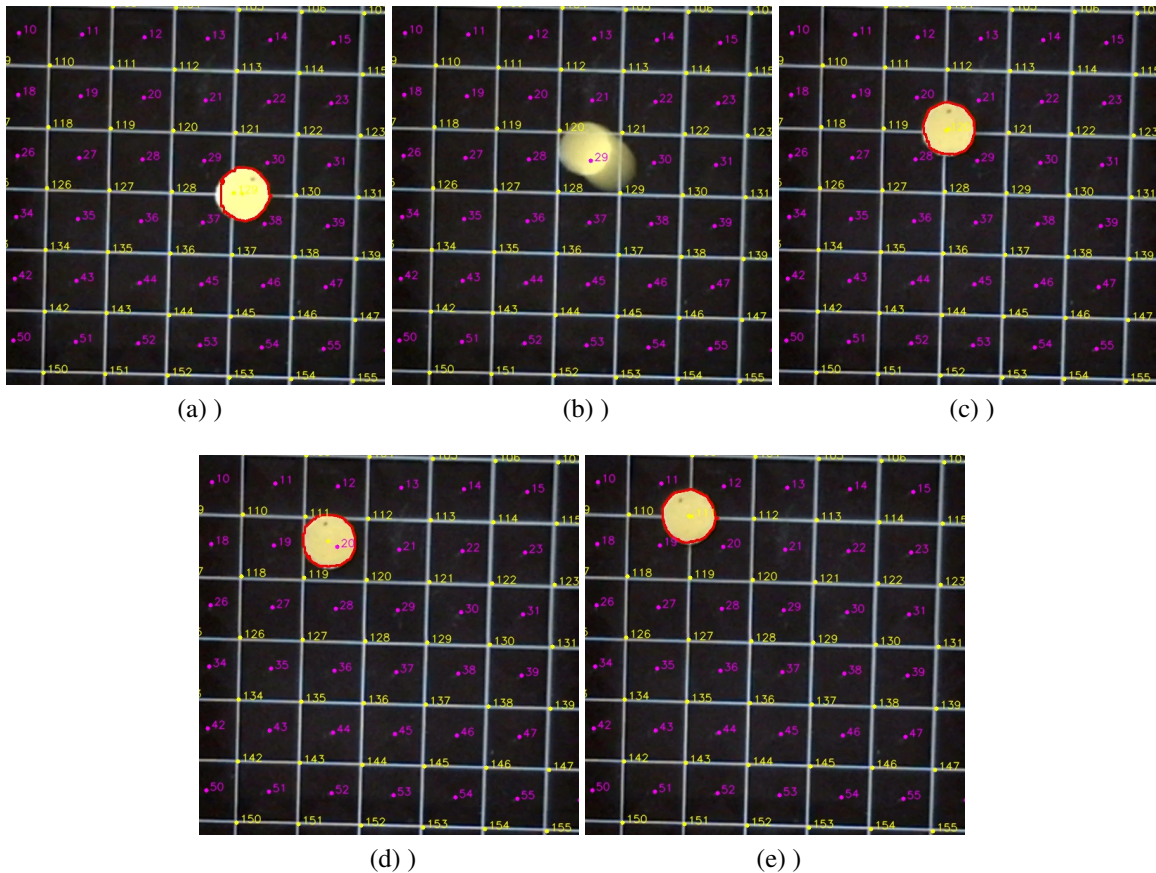


Figure 6.1: Corner to Center movement
Red shaded coil is turned on to repel the robot and yellow shaded coil is turned on to attract

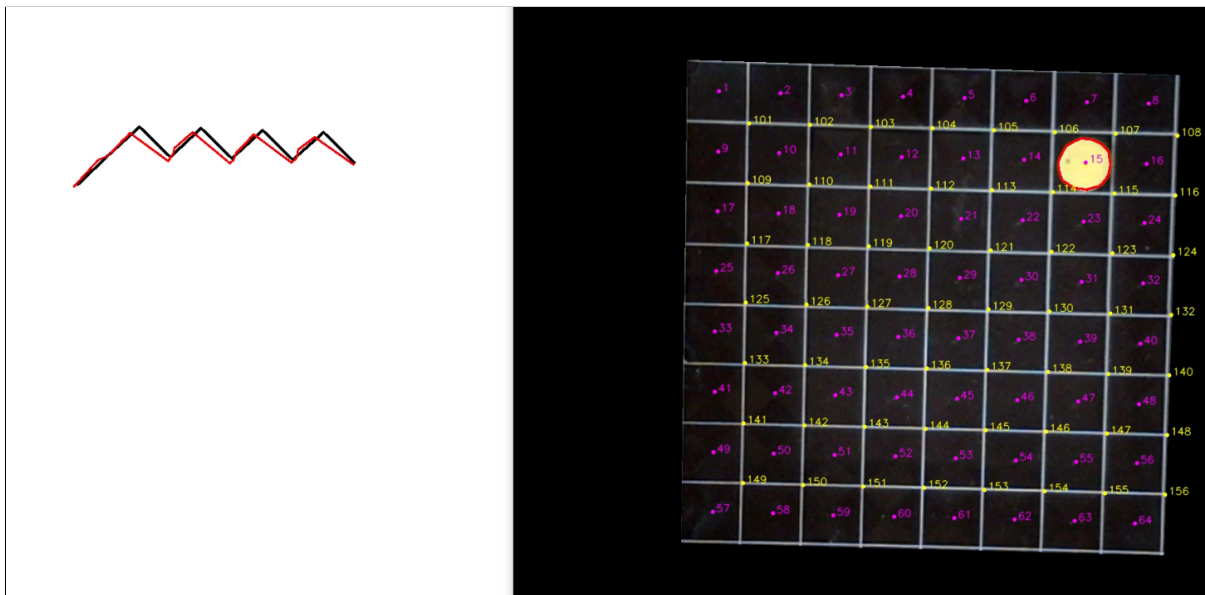


Figure 6.2: Coils required to attract the robot towards the corner.
Green coil- Attractive field, Red coil- Repulsive field. Planned Path- Black, Actual Path- Red

6.2 Multi Robot Manoeuvring experiments

Subsequent experiments to maneuver two robots simultaneously were carried out. The robots were distinguished using color. Path planning algorithm took care so that both robots stay apart from the path of each other. Figure 6.4 shows two robot movements, the expected and actual path traversed.

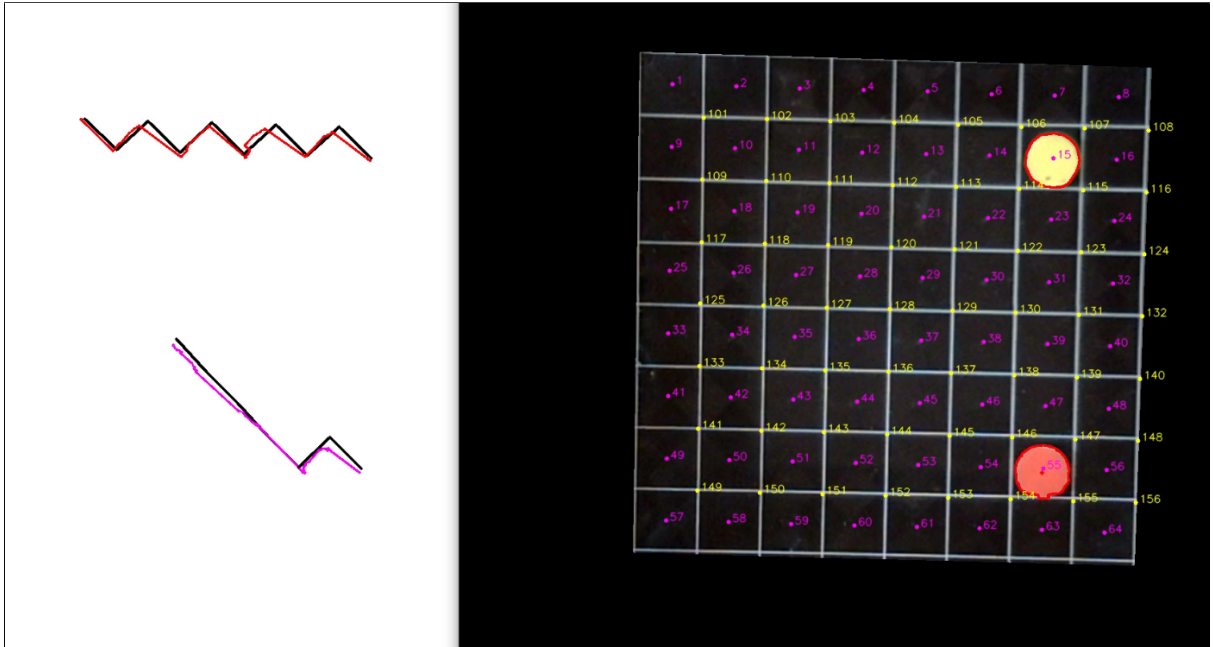


Figure 6.3: Coils required to attract the robot towards the corner.
Green coil- Attractive field, Red coil- Repulsive field

6.3 Application- Part re-orientation

Finally, an attempt was made to perform part re-orientation. A non-magnetic part in the shape of an arrow was used. The angle was calculated using Principal component analysis. The robots were used to push the part in a specific part changing the angle. An attempt was made to use two robots to move as a couple and produce re-orientation. This part was not successful. The figure shows part re-orientation with a single robot. The initial and final angles could be seen to change

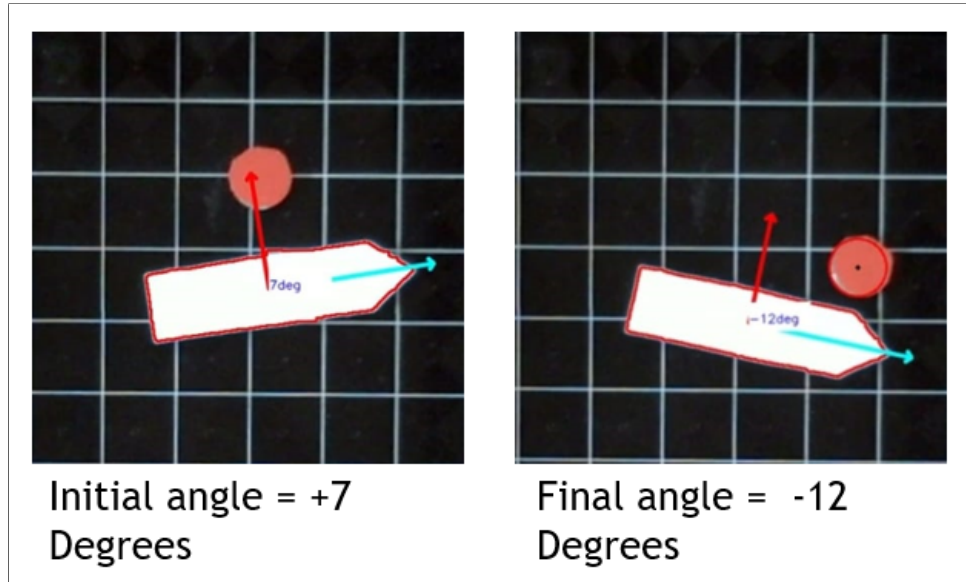


Figure 6.4: Initial and final picture of part-reorientation experiment

Chapter 7

FUTURE WORK

1. The size of the coils can be further reduced to match the size of the micro robots.
2. Force-based feedback- Finding out the required amount of force to send the bot to the next location, and determining the current to be sent through different coils.
3. Integrating Electronic Setup with the PCB, to make the system more compact. Flexible PCBs instead of a Rigid to achieve maneuvering on flexible platforms.
4. The bot can be designed in a way to achieve torque control, which helps in orienting the bot in the same place.

Chapter 8

REFERENCE- GitHub Link

Following material is uploaded

1. Python Codes for Robot image processing
2. Python- Part orientation code
3. Arduino- Main code for python and coil communication
4. Arduino- Coil testing code
5. Matlab- Design Scripts
6. Matlab- Simulink Models
7. Setup Images
8. Experiemnt videos
9. Reference material

Link- [Repository Link](#)

If link is not clickable, visit here

<https://github.com/sameerpuj05/Manoeuvring-of-Micro-Robots-using-External-Magnetic-Fields>

Bibliography

- [1] W Hu J Giltinan M Turan S Yim E Diller M Sitti, H Ceylan. Biomedical applications of untethered mobile milli/microrobots. *Proceedings of the IEEE*, 103(2):205–224, February 2015.
- [2] J. A. Gaines G. Yang and B. J. Nelson. A supervisory wafer-level 3d microassembly system for hybrid mems fabrication. *Journal of Intelligent and Robotic Systems*, 37(1):43–68, 2003.
- [3] D. O. Popa and H. E. Stephanou. Micro and mesoscale robotic assembly. *Journal of manufacturing processes*, 6(1):52–71, 2004.
- [4] I. K. Kaliakatsos B. J. Nelson and J. J. Abbott. Microrobots for minimally invasive medicine. *Annual review of biomedical engineering*, 12:55–85, 2010.
- [5] W. Gao L. Zhang J. Li, B. E.-F. de A vila and J. Wang. Micro/nanorobots for biomedicine: Delivery, surgery, sensing, and detoxification. *Science Robotics*, 2(4), 2017.
- [6] R. M. T. II S. Washburn O. J. Sul, M. R. Falvo and R. Superfine. Thermally actuated untethered impact-driven locomotive microdevices. *Applied Physics Letters*, 89(20):203512, 2006.
- [7] R. Jeong-Hoon R. Polcawich K. Oldham, R. Choong-Ho and J. Pulskampe. Lateral thin-film piezoelectric actuators for bio-inspired micro-robotic locomotion. In *Proceedings of the ASME 2009 International Design Engineering Technical Conferences Computers and Information in Engineering Conference*, San Diego, CA, USA 2009.
- [8] J Zemánek. Distributed manipulation by controlling force fields through arrays of actuators. Prague 2018.
- [9] B. Behkam and M. Sitti. Design methodology for biomimetic propulsion of miniature swimming robots. *Journal of Dynamic Systems, Measurement, and Control*, 128(1):36–43, 2006.
- [10] H. Chen and D. Sun. Moving groups of microparticles into array with a robot tweezers manipulation system. *IEEE Transactions on Robotics*, 28(5):1069–1080, Oct 2012.
- [11] S. Floyd C. Pawashe and M. Sitti. Modeling and experimental characterization of an untethered magnetic micro-robot. *The International Journal of Robotics Research*, 28(8):1077–1094, 2009.

- [12] B. E. Kratochvil R. Borer A. Sengul M. P. Kummer, J. J. Abbott and B. J. Nelson. Octomag: An electromagnetic system for 5-dof wireless micromanipulation. *Robotics, IEEE Transactions*, 26(6):1006–1017, 2010.
- [13] C. Pawashe E. Diller, S. Floyd and M. Sitti. Control of multiple heterogeneous magnetic microrobots in two dimensions on nonspecialized surfaces. *IEEE Transactions on Robotics*, 28(1):172–182, 2012.
- [14] B. E. Kratochvil K. Vollmers, D. R. Frutiger and B. J. Nelson. Wireless resonant magnetic microactuator for untethered mobile microrobots. *Applied Physics Letters*, 92(14):144103, 2008.
- [15] G. Z. Lum Z. Ye E. Diller, J. Giltinan and M. Sitti. Six-degree-of-freedom magnetic actuation for wireless microrobotics. *The International Journal of Robotics Research*, 35(1-3):114–128, 2016.
- [16] M. Sitti. Mobile microrobotics. intelligent robotics and autonomous agents series. *MIT Press*, 2017.
- [17] C. Pawashe S. Floyd and M. Sitti. An untethered magnetically actuated micro- robot capable of motion on arbitrary surfaces. *In Robotics and Automation, 2008. ICRA 2008. IEEE International Conference*, 35(-3):419–424, 2008.
- [18] Color based object tracking with opencv - a survey.
- [19] Circle detection using opencv — python - geeksforgeeks.
- [20] Yiannis Kantaros. Control of magnetic microrobot teams for temporal micromanipulation tasks. Purdue University, 2018.